Iron “Ore” Nothing: Benthic iron fluxes from the oxygen-deficient Santa Barbara Basin enhance phytoplankton productivity in surface waters

De’Marcus Robinson[1*], Anh L.D. Pham[1], David J. Yousavich[2], Felix Janssen[3], Frank Wenzhöfer[3], Eleanor C. Arrington[4], Kelsey M. Gosselin[5], Marco Sandoval-Belmar[1], Matthew Mar[1], David L. Valentine[4], Daniele Bianchi[1], Tina Treude[1,2*]

[1]Department of Atmospheric and Oceanic Sciences, University of California Los Angeles, Los Angeles, CA, USA

[2]Department of Earth, Planetary, and Space Sciences, University of California Los Angeles, Los Angeles, CA, USA

[3]HGF-MPG Joint Research Group for Deep-Sea Ecology and Technology, Alfred Wegener Institute, Helmholtz Centre for Polar and Marine Research, Bremerhaven, Germany

[4]Department of Earth Science and Marine Science Institute, University of California, Santa Barbara, CA 93106, USA

[5]Interepartment Graduate Program in Marine Science, University of California, Santa Barbara, CA 93106, USA

*Correspondence: De'Marcus Robinson, demarcus1.robinson@atmos.ucla.edu; Tina Treude, ttreude@g.ucla.edu

Abstract

The trace metal iron (Fe) is an essential micronutrient that controls phytoplankton productivity, which subsequently affects organic matter cycling with feedback on the cycling of macronutrients. Along the continental margin of the U.S. West Coast, high benthic Fe release has been documented, in particular from deep anoxic basins in the Southern California Borderland. However, the influence of this Fe release on surface primary production remains poorly understood. In the present study from the Santa Barbara Basin, in-situ benthic Fe fluxes were determined along a transect from shallow to deep sites in the basin. Fluxes ranged between 0.23 and 4.9 mmol m^{-2} d^{-1}, representing some of the highest benthic Fe fluxes reported to date. To investigate the influence of benthic Fe release from the oxygen-deficient deep basin on surface phytoplankton production, we combined benthic flux measurements with numerical simulations using the Regional Ocean Model System coupled to the Biogeochemical Elemental Cycling model (ROMS-BEC). For this purpose, we updated the model Fe flux parameterization to include the new benthic flux measurements from the Santa Barbara Basin. Our simulations suggest that benthic Fe fluxes enhance surface primary production, supporting a positive feedback on benthic Fe release by decreasing oxygen in bottom waters. However, a reduction of phytoplankton Fe limitation by enhanced benthic fluxes near the coast may be partially compensated by increased nitrogen limitation further offshore, limiting the efficacy of this positive feedback.

Deleted: existing

Deleted: fluxes

Deleted: simulation suggests

Deleted: iron

Deleted: support

Deleted: creating

Deleted: enhancing low

Deleted: conditions

Deleted: the easing

Deleted: reducing

1. Introduction

The California Current System (CCS), located off the coasts of Washington, Oregon, and California, is a typical Eastern Boundary Upwelling System, where seasonal upwelling supports a highly diverse and productive marine ecosystem (Chavez and Messié, 2009; Carr and Kearns, 2003). The CCS can be split into three main parts: the main equatorward California Current offshore, a subsurface poleward undercurrent fringing the continental shelf, and a recirculation pattern known as the Southern California Eddy in the Southern California Bight.

In the CCS, both upwelling and large-scale circulation provide essential nutrients to the euphotic zone, where they fuel high rates of net primary production (NPP). While seasonal upwelling dominates north of Point Conception, advection by the CCS provides a major route for nutrient supply to the Santa Barbara Channel in the Southern California Bight (Bray et al., 1999). Following phytoplankton blooms, sinking and degradation of organic matter lead to oxygen consumption and widespread oxygen loss in subsurface waters (Brander et al., 2017; Chavez and Messié, 2009). Along the southern California coast, this oxygen depletion is exacerbated by regional circulation patterns that include transport of low-oxygen waters of tropical origin along the poleward undercurrent (Evans et al., 2020; Pozo Buil and Di Lorenzo, 2017). Oxygen decline is particularly apparent in deep, isolated basins such as those found in the Southern California continental borderland, where the presence of shallow sills limits ventilation of deep waters, and anoxic conditions are often encountered near the bottom (Reimers et al., 1990; Goericke et al., 2015; White et al., 2019).

In the CCS, the trace metal iron (Fe) has been identified as a limiting factor for the growth of phytoplankton (Hogle et al., 2018). Fe is an essential micronutrient that has also a considerable influence on the dynamics of phosphorus and nitrogen in the euphotic zone (Tagliabue et al., 2017). Similar to other nutrients, Fe is transported to the surface by upwelling and circulation. However, Fe supply is generally low in oxygenated environments relative to other macronutrients, reflecting rapid scavenging of insoluble iron-oxide minerals by sinking particles that eventually accumulate in the sediment (Bruland et al., 2001, 2014; Firme et al., 2003; Till et al., 2019). While early studies suggested that Fe inputs to the CCS are dominated by rivers and aeolian deposition (Biller and Bruland, 2013; Johnson et al., 2003), more recent work highlights a combination of sources,

Deleted: (Chavez and Messié, 2009; Carr and Kearns, 2003)

Deleted: (Evans et al., 2020; Pozo Buil and Di Lorenzo, 2017)

Field Code Changed

Deleted: In the CCS, the trace metal iron (Fe) has been identified as a limiting factor for the growth of phytoplankton (Hogle et al., 2018). Fe is an essential micronutrient that has also a considerable influence on the dynamics of phosphorus and nitrogen in the euphotic zone (Tagliabue et al., 2017). Similar to other nutrients, Fe is transported to the surface by upwelling and circulation, but the supply is generally low in an oxic environment relative to other macronutrients, reflecting rapid scavenging of the insoluble iron-oxide minerals by sinking particles that eventually accumulate in the sediment (Bruland et al., 2001, 2014; Firme et al., 2003; Till et al., 2019). While early studies suggested that Fe inputs to the CCS are dominated by rivers and aeolian deposition (Biller and Bruland, 2013; Johnson et al., 2003), more recent work highlights a combination of sources, including benthic fluxes (Severmann et al., 2010; Noffke et al., 2012; Tagliabue et al., 2017) and ocean currents, in redistributing Fe in coastal waters (Bray et al., 1999; Boiteau et al., 2019; García-Reyes and Largier, 2010).¶
Importantly, benthic release of Fe(II), the reduced and soluble form of Fe, has been recognized as a potential source of Fe to the surface ocean along the continental shelf and slope of the CCS, including the deep basins of the California borderland (John et al., 2012; Severmann et al., 2010). Under hypoxic or anoxic bottom water conditions, Fe(II) produced in the sediment during microbial organic matter degradation coupled to Fe (III) reduction diffuses across the sediment-water interface and accumulates in the water column (Furrer and Wehrli, 1993; Dale et al., 2015; Severmann et al., 2010). In the CCS, this benthic Fe flux is likely to exceed atmospheric deposition (Deutsch et al., 2021a), and may ultimately make its way to the surface by upwelling and vertical mixing, supporting high rates of photosynthesis. ¶
The interaction between low bottom water oxygen, Fe(II) release, and transport by the ocean circulation are particularly important in the Santa Barbara Basin (SBB), an oxygen-deficient basin located between the Channel Islands and mainland California in the Southern California Bight. The SBB frequently experiences seasonal anoxia in the bottom water in fall, with irregular oxygen flushing of dense, hypoxic water below the western sill depth (470 m) during winter and spring (Goericke et al., 2015; Sholkovitz and Soutar, 1975; White et al., 2019). This seasonal flushing reflects either changes in upwelling strength and frequency, or changes in stratification at the sill depth, although the exact cause of the flushing is still unclear (Goericke et al., 2015; Sholkovitz and Gieskes, 1971; White et al., 2019). Lack of oxygen in the deeper parts of the basin support anaerobic microbial processes in the bottom water and sediment (White et al., 2019), including benthic Fe reduction (Goericke et al., 2015) causing the release of Fe(II) into the water column (Severmann et al., 2010). Ventilation events that re-oxygenate the deep basin, as well as mixing by the vigorous submesoscale circulation (Kessouri et al., 2020) could allow upwelling of this Fe above the sill depth and ultimately to the surface, providing a linkage between benthic processes ... [1]

including benthic fluxes (Severmann et al., 2010; Noffke et al., 2012; Tagliabue et al., 2017; Wallmann et al., 2022) and ocean currents, which help redistributing Fe in coastal waters (Bray et al., 1999; Boiteau et al., 2019; García-Reyes and Largier, 2010).

Benthic release of Fe(II), the reduced and soluble form of Fe, has been recognized as a potential source of Fe to the surface ocean along the continental shelf and slope of the CCS, including the deep basins of the California borderland (John et al., 2012; Severmann et al., 2010). Under hypoxic or anoxic bottom waters, Fe(II) produced in the sediment during microbial organic matter degradation coupled to Fe (III) reduction diffuses across the sediment-water interface and accumulates in the water column (Furrer and Wehrli, 1993; Dale et al., 2015; Severmann et al., 2010; Wallmann et al., 2022). In the CCS, this benthic Fe flux is likely to exceed atmospheric deposition (Deutsch et al., 2021), and may ultimately make its way to the surface by upwelling and vertical mixing, supporting high rates of photosynthesis.

The interaction between low bottom water oxygen, Fe(II) release, and transport by the ocean circulation is particularly important in the Santa Barbara Basin (SBB), an oxygen-deficient basin located between the Channel Islands and mainland California in the Southern California Bight. The SBB frequently experiences seasonal anoxia in the bottom water in fall, with irregular oxygen flushing of dense, hypoxic water below the western sill depth (470 m) during winter and spring (Goericke et al., 2015; Sholkovitz and Soutar, 1975; White et al., 2019; Qin et al., 2022). This seasonal flushing reflects either changes in upwelling strength and frequency, or changes in stratification at the sill depth, although the exact cause of the flushing is still unclear (Goericke et al., 2015; Sholkovitz and Gieskes, 1971; White et al., 2019). Lack of oxygen in the deeper parts of the basin supports anaerobic microbial processes in the bottom water and sediment (White et al., 2019), including benthic Fe reduction (Goericke et al., 2015), causing the release of Fe(II) into the water column (Severmann et al., 2010). Ventilation events that re-oxygenate the deep basin, as well as mixing by the vigorous submesoscale circulation (Kessouri et al., 2020), could allow upwelling of this Fe above the sill depth and ultimately to the surface, providing a linkage between benthic processes and upper water-column biogeochemistry. Increased surface primary production supported by this Fe source would in turn drive higher remineralization and oxygen loss in deep waters, thus providing a positive feedback to benthic Fe release. However, with a dearth of benthic Fe flux measurements in the SBB, gaps remain in our understanding of the dynamics and impact

of benthic Fe flux in the Southern California Borderland, particularly with respect to its magnitude, dependence on bottom water oxygen, and ability to reach the euphotic zone and influence primary production.

In this study, we explore the connection between benthic Fe flux and surface primary production in the CCS, by investigating the influence of enhanced benthic Fe fluxes from low-oxygen waters with a combination of field observations and experiments with a numerical model. We focus on the SBB, where we provide a new set of benthic Fe flux estimates determined by in-situ benthic flux chamber measurements. We combine these new observations with existing data (Severmann et al., 2010) to revise the representation of benthic Fe fluxes in UCLA's Regional Ocean Modeling System coupled to the Biogeochemical Elemental Cycling (ROMS-BEC) model (Deutsch et al., 2021). We then use the model to evaluate the effect of benthic Fe fluxes on surface nutrient consumption and NPP, and compare their impact to that of aeolian Fe deposition in the SBB and beyond.

2. Materials and Methods

2.1 Study Site

Fieldwork in the SBB was conducted between Oct 29 and Nov 11, 2019, during the R/V Atlantis cruise AT42-19. Sampling occurred during the anoxic, non-upwelling season along one bimodal transect with six stations total at depths between 447 and 585 m (**Fig. 1, Table 1**).

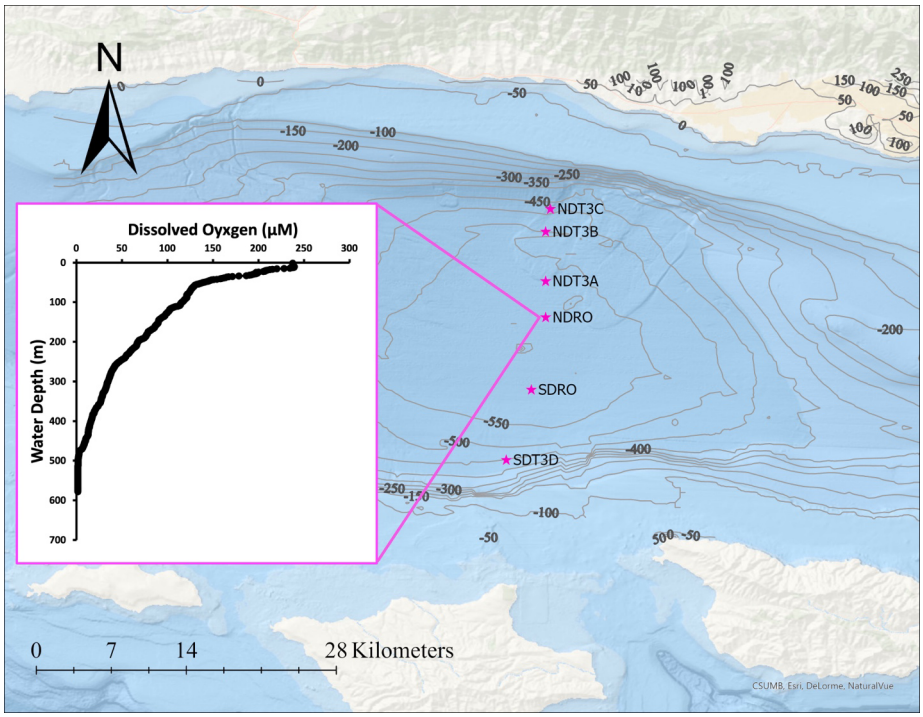

Figure 1. Station locations in the SBB during the AT42-19 expedition with R/V Atlantis. NDT3 (with stations A, B, C) = Northern Depocenter Transect Three, NDRO = Northern Depocenter Radial Origin, SDRO = Southern Depocenter Radial Origin, SDT3 (with station D) = Southern Depocenter Transect Three. The small insert figure displays dissolved oxygen concentrations in the water column at the NDRO station profiled by an optical oxygen sensor attached to the AUV

Deleted: accomplished

Deleted: transects

Deleted: The map in **Fig. 1** was created using ArcGIS Ocean Basemap. The GEBCO bathymetric data source was used to add contour lines.

Deleted: North

Deleted: optode

Sentry. The profile was measured at the following position: Latitude 34.2618 N, Longitude -120.0309 E. The map was created using ArcGIS Ocean Basemap, with bathymetric contour lines representing depth information taken from the General Bathymetric Chart of the Ocean (GEBCO) database.

Transects were divided into northern (NDT3 = Northern Depocenter Transect Three) and southern (SDT3 = Southern Depocenter Transect Three) sites based on basin geography (**Fig. 1**). Stations were labeled alphabetically from A (deepest) to D (shallowest) according to their location along the transect, except for the deepest stations at the bottom of the basin, which were labeled Northern Depocenter Radial Origin (NDRO) and Southern Depocenter Radial Origin (SDRO).

2.2 Benthic Flux Chambers

Custom-built cylindrical benthic flux chamber systems (Treude et al., 2009) were deployed by the ROV Jason at the six stations (**Fig. 1**). Polycarbonate chambers (19 cm inner diameter) were installed in a small lightweight frame made from fiber-reinforced plastics. A stirrer (Type K/MT 111, K.U.M. Umwelt- und Meerestechnik, Kiel, Germany) was used to keep the water overlying the sediment enclosed by the chamber well mixed. One or two replicate chamber systems were deployed at each site. Since sediment in the SBB is quite soft and poorly consolidated, especially towards the deeper stations, frames were fitted with platforms attached to the feet of the frame and with buoyant syntactic foam to reduce sinking into the sediment. A syringe sampler was equipped with 6 glass sampling syringes that were connected with 50 cm long plastic tubes (2.5mm inner diameter, Vygon, Aachen, Germany). Each sampling syringe withdrew 50 mL of the overlying seawater at pre-programmed times. A seventh syringe was used to inject 50 mL of de-ionized water shortly after chambers were deployed to calculate chamber volume from the salinity-drop recorded with a conductivity sensor (type 5860, Aanderaa Data Instruments, Bergen, NO) in the overlying water, following the approach described in (Kononets et al., 2021). Water samples were analyzed for Fe(II) on the ship using a Shimadzu UV-Spectrophotometer (UV-1800), equipped with a sipper unit, following the procedure of (Grasshoff and Ehrhardt, 1999). Fe fluxes were calculated from the slope of linear fits of Fe concentration time series vs. time (**Fig. S1**), multiplied by the chamber volume, and divided by the surface area of the sediment (Kononets et al., 2021).

2.3 Numerical model (ROMS-BEC)

Deleted: , Longitude -120.0309.

Deleted: North

Deleted: Custom-built cylindrical benthic flux chambers (Treude et al., 2009) were deployed by the ROV Jason at the indicated stations (**Fig. 1**). Chambers were installed in a small lightweight frame made from fiber-reinforced plastics. A stirrer was used to keep the water overlying the sediment enclosed by the chamber well mixed. One or two replicate chambers were deployed at each site. Since sediment in the SBB is quite soft and poorly consolidated, especially towards the deeper stations, frames were fitted with platforms attached to the feet of the frame and with buoyant syntactic foam to reduce sinking into the sediment. A syringe sampler equipped with 6 glass sampling syringes withdrew 50 mL of the overlying seawater at pre-programmed times. A seventh syringe was used to inject 50 mL of de-ionized water shortly after chambers were deployed to calculate chamber volume from the salinity-drop recorded with a conductivity sensor (type 5860, Aanderaa Data Instruments, Bergen, NO) in the overlying water, following the approach described in (Kononets et al., 2021). Water samples were analyzed for Fe(II) on the ship using a Shimadzu UV-Spectrophotometer (UV-1800), equipped with a sipper unit, following the procedure of (Grasshoff and Ehrhardt, 1999). Fe fluxes were calculated from the slope of linear fits of Fe concentration time series vs. time (**Fig. S1**), multiplied by the chamber volume, and divided by the surface area of the sediment (Kononets et al., 2021).¶

2.3 Numerical model (ROMS-BEC)¶

To explore the impacts of benthic Fe fluxes on surface primary production, we used a well-established ocean biogeochemical model of the CCS (Renault et al., 2016; Deutsch et al., 2021a). The physical model component consists of the Regional Ocean Modeling System (ROMS), (Shchepetkin, 2015; Shchepetkin and McWilliams, 2005) a primitive-equation, hydrostatic, topography-following ocean model. As in prior work, the model domain spans the entire U.S. West Coast, from Baja California to Vancouver Island, with a horizontal resolution of 4 km, enough to resolve the mesoscale circulation (Capet et al., 2008). The baseline model configuration was run over the period 1995–2017 with interannually varying atmospheric forcings. We refer the reader to earlier publications (Renault et al., 2021; Deutsch et al., 2021a) for a complete description of the model configuration, setup, forcings and boundary conditions used in this study.¶

ROMS is coupled online to the Biogeochemical Elemental Cycling (BEC) model (Moore et al., 2004), adapted for the U.S. West Coast by (Deutsch et al., 2021b). BEC solves the equations for the evolution of six nutrients (nitrate (NO_3^-), ammonium (NH_4^+), nitrite (NO_2^-), silicate (SiO_2), phosphate (PO_4^{3-}), and iron (Fe)), three phytoplankton groups (small phytoplankton, diatoms, and diazotrophs), a single zooplankton group, inorganic carbon, oxygen, and dissolved organic matter (carbon, nitrogen, phosphorus, and iron). Nutrient and carbon cycles are coupled by a fixed stoichiometry, except for silica and Fe, which use variable stoichiometries (Deutsch et al., 2021a; Moore et al., 2001, 2004). The Fe cycle in BEC includes four separate pools: dissolved inorganic Fe (dFe), dissolved and particulate organic Fe, and Fe associated with mineral dust. Of thes ... [2]

To explore the impacts of benthic Fe fluxes on surface primary production, we used a well-established ocean biogeochemical model of the CCS (Renault et al., 2016; Deutsch et al., 2021). The physical model component consists of the Regional Ocean Modeling System (ROMS), (Shchepetkin, 2015; Shchepetkin and McWilliams, 2005) a primitive-equation, hydrostatic, topography-following ocean model. As in prior work, the model domain spans the entire U.S. West Coast, from Baja California to Vancouver Island, with a horizontal resolution of 4 km, enough to resolve the mesoscale circulation (Capet et al., 2008). The baseline model configuration was run over the period 1995–2017 with interannually varying atmospheric forcings. We refer the reader to earlier publications (Renault et al., 2021; Deutsch et al., 2021) for a complete description of the model configuration, setup, forcings and boundary conditions used in this study.

ROMS is coupled online to the Biogeochemical Elemental Cycling (BEC) model (Moore et al., 2004), adapted for the U.S. West Coast by (Deutsch et al., 2021). BEC solves the equations for the evolution of six nutrients (nitrate (NO_3^-), ammonium (NH_4^+), nitrite (NO_2^-), silicate (SiO_2), phosphate (PO_4^{3-}), and iron (Fe)), three phytoplankton groups (small phytoplankton, diatoms, and diazotrophs), a single zooplankton group, inorganic carbon, oxygen (O_2), and dissolved organic matter (carbon, nitrogen, phosphorus, and iron). Nutrient and carbon cycles are coupled by a fixed stoichiometry, except for silica and Fe, which use variable stoichiometries (Deutsch et al., 2021; Moore et al., 2001, 2004). The Fe cycle in BEC includes four separate pools: dissolved inorganic Fe (dFe), dissolved and particulate organic Fe, and Fe associated with mineral dust. Of these, only dissolved organic and inorganic Fe are explicitly tracked as state variables, while particulate Fe is treated implicitly by resolving vertical sinking particle fluxes (Moore et al., 2001; Moore and Braucher, 2008). Four main processes control the cycle of Fe in the model: atmospheric deposition, biological uptake and remineralization, scavenging by sinking particles, and release by sediment. The atmospheric dFe deposition is based on the dust climatology of (Mahowald et al., 2006), and dissolution rates from (Moore and Braucher, 2008). Different from (Deutsch et al., 2021), we re-evaluated the dependence of benthic dFe fluxes on bottom water O_2 concentrations in the California margin based on a merged dataset that combines our measurements from the SCB, with those presented in (Severmann et al., 2010) (see Section 2.5). The model Fe scavenging scheme removes dFe from the water column at a rate proportional to sinking particle fluxes and dFe concentrations, assuming a uniform concentration of 0.6 nM of Fe-binding ligands (Moore et al., 2004; Moore and Braucher, 2008). Accordingly, scavenging rates increase strongly at dFe

concentrations greater than 0.6 nM, and vice versa rates decrease strongly below 0.5 nM (**Fig. S2**). Note that, while simplistic, this formulation is still widely adopted by global ocean biogeochemistry models (Tagliabue et al., 2014, 2016), although improvements have been proposed (Moore and Braucher, 2008; Aumont et al., 2015; Pham and Ito, 2019, 2018).

As shown in previous work, the model captures the main patterns of physical and biogeochemical variability in the CCS, providing a representation of nutrient cycles and NPP in good agreement with observations (Renault et al., 2021; Deutsch et al., 2021). We further evaluate the model against an extended set of dissolved Fe measurements for the CCS (see Sections **2.4** and **3.1**).

2.4 Fe dataset along the U.S. West Coast

To assess the ability of the model to capture observed patterns in dFe along the U.S. West Coast, we gathered available dFe concentration measurements from published studies, including a global compilation (Tagliabue et al., 2016), regional programs such as CalCOFI, CCE-LTER, IRNBRU and MBARI cruises (Bundy et al., 2016; Hogle et al., 2018; Johnson et al., 2003; King and Barbeau, 2011), and other individual studies (Biller and Bruland, 2013; Boiteau et al., 2019; Bundy et al., 2014, 2015, 2016; Chappell et al., 2019; Chase, 2002; Chase et al., 2005; Firme et al., 2003; Hawco et al., 2021; John et al., 2012; Till et al., 2019). In the final compilation, we define dFe as the sum of the dissolved Fe and dissolvable Fe, based on the definitions used in each publication. Different studies used different filter sizes to define the dFe pool, most commonly 0.20, 0.40, and 0.45 µm, and different sampling methods, such as bottles, pump systems and/or surface tows. In some studies, samples were briefly acidified before being analyzed. Despite the differences in sampling and measurement approaches, we found that these datasets generally agreed with each other, suggesting that the final compilation accurately represents the dFe distribution along the U.S. West Coast. The final dataset includes observations from 1980 to 2021, with most samples collected between 1997 and 2015, and from the upper 100 m of the water column.

2.5 Experimental Design

To evaluate the impact of Fe fluxes from low-O_2 sediment in the SBB on surface biogeochemistry, we designed a suite of model sensitivity experiments with ROMS-BEC in which external sources

Deleted: oxygen

of Fe are modified relative to a baseline simulation. Accordingly, we run the following model experiments:

***High-flux**:* This experiment is the baseline model simulation, using a Fe flux parameterization calculated as an exponential fit to a data set of benthic Fe fluxes consisting of the new benthic measurements from AT42-19 and previous observations from the U.S. West Coast (Severmann et al., 2010) (see Section 3.2), thus updating the parameterization by (Deutsch et al., 2021). Benthic Fe release follows the equation:

$$\log_{10}(\mathrm{Fe}) = 2.86 - 0.01 \cdot O_2 \quad \text{(Equation 1)}$$

Where O_2 is the concentration of oxygen in mmol m^{-3} and (Fe) is the Fe flux in µmol m^{-2} d^{-1}. This revised formulation is only applied in the SBB where we performed our measurements, while a different formulation, solely based on data by (Severmann et al., 2010) is used outside of the SBB:

$$\log_{10}(\mathrm{Fe}) = 2.6178 - 0.0128\ O_2 \quad \text{(Equation 2)}$$

For this parameterization, we corrected a model bias that resulted in modeled bottom O_2 concentrations greater than 30 mmol m^{-3} over most of the deep basins where observations indicated lower concentrations, down to oxygen-free conditions (**Fig. S3**). We therefore reduced modeled bottom water O_2 concentrations in the Southern California Borderland by 30 mmol m^{-3}, based on the average difference between model and observed O_2 in the region. This correction is crucial to producing realistic benthic Fe fluxes under the anoxic conditions observed in the SBB, rather than fluxes at O_2 concentrations of 30 mmol m^{-3}.

Hypoxia-off: The purpose of this experiment is to evaluate the importance of enhanced Fe fluxes under low-O_2 conditions in the SBB. Benthic Fe fluxes are calculated as in *High-flux* experiment (Equation 2), but they are capped at a constant value when O_2 decreased below a threshold of 65 mmol m^{-3}, which we chose as representative of hypoxic conditions (Deutsch et al., 2011). This change is applied only to in the SBB, and effectively bounds the benthic Fe release at 1.48 µmol m^{-2} d^{-1} when O_2 drops below the threshold for hypoxia.

Deleted: ***Control***: This is the baseline model simulation, using the Fe flux parameterization based on the measurements by (Severmann et al., 2010) following the parameterization by (Deutsch et al., 2021b). Fe release follows the equation: ¶
$\log_{10}\Phi(\mathrm{Fe}) = 2.5 - 0.0165 \cdot O_2$ **(Eq. 1)**¶
where O_2 is the concentration of oxygen in mmol m^{-3} and Φ(Fe) is the Fe flux in µmol m^{-2} d^{-1}. Note that this experiment reflects the original Fe flux parameterization in UCLA's ROMS-BEC and does not include information from the Fe flux measurements conducted during AT42-19, which show significantly higher Fe release under anoxic conditions.¶
Low Oxygen Threshold: The purpose of this experiment is to evaluate the importance of enhanced Fe fluxes under low-oxygen conditions in the bottom water. Benthic Fe fluxes are calculated as in *Control*, but capped at a constant value when oxygen decreased below a specific threshold. We performed two "*Low Oxygen Threshold*" model experiments. The first uses an O_2 threshold of 100 µM (***Low Oxygen Threshold-100***), and caps Fe release at 0.85 µmol m^{-2} d^{-1} when oxygen drops below 100 µM. The second uses a threshold of 65 µM (***Low Oxygen Threshold-65***), and caps Fe release at 1.48 µmol m^{-2} d^{-1} when oxygen drops below 100 µM. The 65 µM threshold is close to the typical definition of hypoxia (~60 µM), while the 100 µM threshold was chosen to investigate the general impact of benthic Fe fluxes from low-O_2 coastal sediment, because around 80 % of the shelf in our model is characterized by bottom O_2 concentration lower than 100 µM (**Fig. S3**)¶
High-flux: This simulation investigates the importance of high benthic Fe fluxes in the SBB, and is based on the new benthic measurements from AT42-19 combined with previous observations (Severmann et al., 2010). We derived and applied a new parameterization for the dependence of benthic Fe flux on bottom O_2 using the combined Fe flux dataset: ¶
$\log_{10}\Phi(\mathrm{Fe}) = 2.86 - 0.01 \cdot O_2$ **(Eq. 2)**¶
This revised formulation is only applied in the SBB, while the same formulation as *Control* is used elsewhere. We further corrected a model bias that limits simulations to O_2 concentrations >30 mmol m^3. This correction is crucial to allow the model the estimation of benthic Fe fluxes under anoxic conditions, rather than simulating fluxes at 30 mmol m^3. We therefore applied a constant deduction of 30 mmol O_2 m^{-3} to the model's bottom water O_2 based on the average difference between model and observed O_2 in the SBB.¶

Deleted:

***Dust-off*:** The purpose of this experiment is to evaluate the importance of aeolian Fe deposition in the CCS, and to compare it with the benthic Fe fluxes. In this experiment, the atmospheric Fe deposition is set to zero; all other settings are identical to the *High-flux* experiment.

The baseline (*High-flux*) model simulation is run from 1995 to 2017. The other two model sensitivity experiments (*Hypoxia-off* and *Dust-off)* are branched off from the *High-flux* simulation in year 2008 and run separately for 10 additional years (2008-2017). All model experiments use the same set of forcings and initial conditions. Results from the final 3 years (2015-2017) of the *Hypoxia-off* and *Dust-off* simulations are averaged and analyzed by comparing differences in biogeochemical fields (Fe, NO_3^-, and NPP) to the final 3 years of the *High-flux* run.

Deleted: .

Deleted: *Control*

Formatted: Font: Italic

Deleted: Each

Deleted: experiment is run

Deleted: over a time frame of 6

Deleted: from 2004-2009, using

Deleted: year (2009) are

Deleted: results from the *Control*

3. Results

3.1 In-situ benthic Fe fluxes and model parameterization

Benthic Fe fluxes from in-situ benthic chamber measurements during the AT42-19 expedition are shown in **Table 1**. High Fe flux was recorded at the anoxic depocenter stations (4.90 and 3.92 mmol m^{-2} d^{-1} at SDRO and 3.49 mmol m^{-2} d^{-1} at NDRO). Fe fluxes at the shallower hypoxic stations (NDT3C, NDT3B, and SDT3D) were an order of magnitude lower. The Fe flux at the hypoxic NDT3A station between NDRO and NDT3B was approximately half the flux observed at the depocenter.

Table 1. Station details and geochemical parameters determined during the AT42-19 expedition. Benthic Fe fluxes were determined using in-situ benthic chambers. Dissolved O_2 concentrations were measured in the water column at 10 m above the seafloor using a Seabird optode sensor attached to the ROV Jason. At stations with two benthic chamber deployments (NDT3A and SDRO), O_2, geographical coordinates, and depth were averaged as there were only minimal differences between the two chamber deployments.

Station	Fe Flux [mmol m^{-2} d^{-1}]	O_2 [mmol m^{-3}]	Latitude [N]	Longitude [E]	Depth [m]
NDT3C	0.23 (n=1)	5.3	34.3526	-120.0160	499
NDT3B	0.36 (n=1)	6.8	34.3336	-120.0188	535
NDT3A	1.73; 1.20 (n=2)	9.6	34.2921	-120.0258	572
NDRO	3.49 (n=1)	0.0	34.2618	-120.0309	581
SDRO	4.90; 3.92 (n=2)	0.0	34.2011	-120.0446	586
SDT3D	0.58 (n=1)	9.6	34.1422	-120.0515	446

Trends in the Fe fluxes suggest modulation by O_2 concentration, water depth, and/or bathymetry. We also note that observed oxygen concentration represents a snapshot of bottom water conditions, while Fe fluxes likely reflect the oxygenation history at any given site. We observed a decrease in the Fe flux with a decrease in water depth (**Fig. 2**). There was also a slight trend of higher Fe fluxes

Deleted: in comparison.
Deleted: of
Formatted: Font: 12 pt
Deleted: oxygen
Formatted: Font: 12 pt
Deleted: sensors
Formatted: Font: 12 pt
Deleted: ,
Formatted: Font: 12 pt
Deleted: Oxygen¶ [µM
Deleted Cells
Formatted: French
Formatted Table
Deleted: oxygen
Deleted: .

with lower O_2 concentrations (most pronounced when O_2 reaches zero); however, since O_2 concentrations were relatively low at all stations (<10 mmol m^{-3}) it is difficult to distill a clear pattern based on the small dataset. Notably, the NDT3A station showed a high Fe flux despite exhibiting the same O_2 concentration as the shallower station SDT3D. Basin bathymetry may also contribute to observed differences in the flux. For instance, the deeper depocenter and A-station showed higher averaged fluxes than the B, C, and D stations**.** We further noticed differences between the north and south extension of the transect. The southern stations (SDRO and SDT3D) showed a higher Fe flux than the northern stations (NDRO and NDT3C).

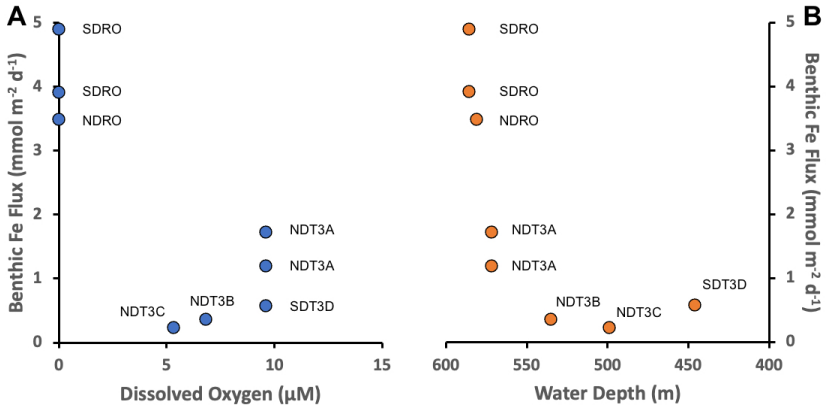

Figure 2. Benthic in-situ Fe fluxes. A: Fluxes as a function of O_2. B: Fluxes as a function of (station) water depth. Note that water depth is shown from deep to shallow depths. See Table 1 for station details.

We combined Fe fluxes determined during AT42-19 with previous estimates along the CCS, as compiled by (Severmann et al., 2010), and analyzed them as a function of bottom water O_2 (**Fig. 3**). Pooled together, the measurements can be described reasonably well by an exponential increase of Fe fluxes with declining bottom water O_2 (Severmann et al., 2010), although significant variability around an exponential fit remains. This relationship is consistent with the Fe flux parameterization adopted in the ROMS-BEC model (Deutsch et al., 2021). Several observations from the AT42-19 cruise (red dots in **Fig. 3**) exceed the range of previous measurements (blue

Deleted: oxygen

Deleted: oxygen

Deleted: µM

Deleted: oxygen

Deleted: oxygen

Deleted: in reverse order. For

Deleted: see Table 1

Deleted: We combined Fe fluxes determined during AT42-19 with previous determinations along the CCS, as compiled by (Severmann et al., 2010), and analyzed them as a function of bottom water oxygen (**Fig. 3**). Pooled together, the measurements can be well described by an exponential increase of Fe fluxes with declining bottom water oxygen (Severmann et al., 2010), consistent with the Fe flux parameterization adopted in the ROMS-BEC model (Deutsch et al., 2021b). Several observations from the AT42-19 cruise (red dots in **Fig. 3**) exceed the range of previous measurements (yellow dots in **Fig. 3**), likely owing to the anoxic or near-anoxic conditions in the water. Relative to the exponential fit to the dataset by (Severmann et al., 2010) (green line in **Fig. 3**) the revised fit to the pooled data (purple line in **Fig. 3**) expands Fe fluxes by approximately two times at oxygen concentrations near zero, and up to one order of magnitude at concentrations near 100 µM.¶

dots in **Fig. 3**), likely owing to the anoxic or near-anoxic conditions in the water. Relative to the exponential fit to the dataset by (Severmann et al., 2010) (yellow line in **Fig. 3**, see Equation 2) the revised fit to the pooled data (purple line in **Fig. 3**, see Equation 1) expands Fe fluxes by approximately a factor of two at O_2 concentrations close to zero, but decreases the magnitude of the Fe fluxes at concentrations above approximately 130 mmol m^{-3}.

3.2 Model evaluation: High flux simulation

The *High-flux* simulation captures the magnitude and patterns of the observed dFe distribution in the upper ocean (**Fig. 4**), consistently with our knowledge of the ocean Fe cycle. In both model and observations, dFe concentrations are low at the surface, as a result of phytoplankton uptake, and increase gradually in subsurface waters due to organic matter remineralization in the water column and at the seafloor, and benthic Fe fluxes from the sediment **(Fig. S4)**. The highest dFe concentrations are found along the coast, likely related to high surface productivity and shallow carbon export and remineralization, combined with basin bathymetry and O_2 deficiency. In the open ocean, dFe concentrations are low in both model and observations, reflecting a combination of phytoplankton uptake, scavenging by sinking particles, and low external inputs.

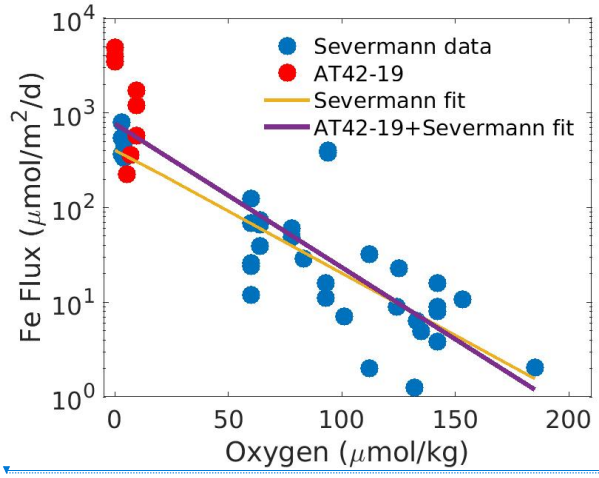

Deleted: *Control*

Deleted: because

Formatted: Font: Bold

Formatted: Font: Bold

Deleted: oxygen

Formatted: Font: Not Bold

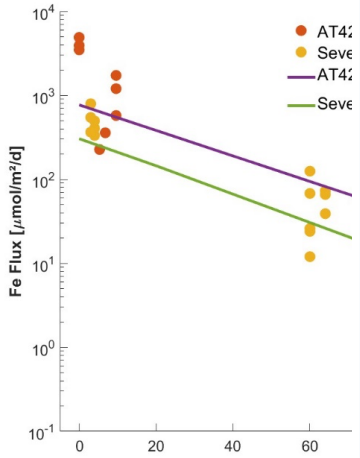

Deleted:
Figure 3. Combined Fe flux data as a function of oxygen. Fe flux data from (Severmann et al., 2010) (orange dots) were fitted with a line of best fit (green) as the original model parametrization. AT42-19 (red dots) were fitted along a line of best fit (purple) that includes Severmann's data point

... [3]

Figure 3. Combined benthic Fe flux data as a function of bottom oxygen. Blue dots show data from the compilation by (Severmann et al., 2010); red dots measurements from the AT42-19 cruise. The yellow line shows an exponential fits to the dataset by (Severmann et al., 2010) (Equation 2). The purple line shows an exponential fit to the combined dataset (Equation 1). Note the logarithmic scale used for the y-axis.

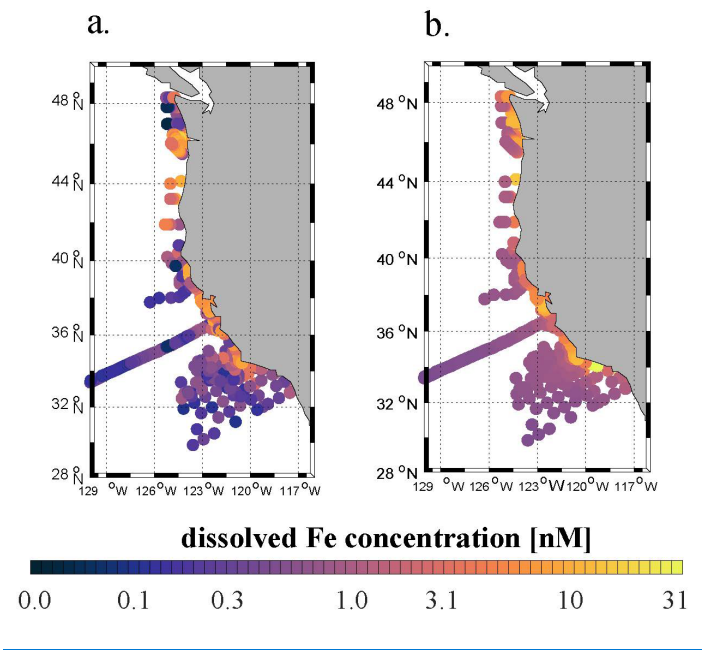

Figure 4. (a) Observed dFe concentrations (nM) from the U.S. West Coast compilation (see Section **2.4**) averaged between 0 and 100 m depth. (b) Annual mean modeled dFe concentrations (nM) averaged between 0 and 100 m depth, sampled at the same locations as the observations in panel (a).

Observational limitations prevent a more detailed validation of subsurface dFe patterns. Measurements of dFe concentrations in subsurface and deep waters (> 100 m) are currently very sparse in the CCS region and Southern California Borderland. Most of the dFe measurements for

Formatted: Font: Not Bold

Deleted: section

Deleted: Modeled annual

Formatted: Font: Bold

Deleted: (note that

Deleted: are identical to (a)).

Deleted: The agreement of the model dFe with observations (R=0.5, **Fig. 4b**) reflects results from other ocean models compiled in (Tagliabue et al., 2016). However, the model tends to underestimate the sharp dFe gradient between coastal and open ocean waters, overestimating dFe in the open ocean and producing too uniform concentrations offshore and at depth (**Fig. 4; Fig. S4**). These biases are likely related to the simple Fe scavenging scheme, which assumes a constant Fe-binding ligand concentration of 0.6 nM. The low number and episodic nature of in-situ measurements may also explain some of the mismatch between model and observations. ¶
At the scale of the CCS, the *Control* simulation produces lower surface dFe in the southern domain (33 - 36°N), and higher surface concentration in the northern domain (40 - 45°N) and near the central coast (**Fig. 5a**). While these patterns reflect a combination of internal Fe cycling and external inputs, the elevated dFe in the northern part of the CCS, in particular offshore, can be partly attributed to higher aeolian deposition in that region (**Fig. S5**) as well as coastal inputs from the Juan De Fuca strait (Deutsch et al., 2021b). ¶
Relative to Fe, NO_3^- shows fewer variable patterns along the meridional direction, and a more pronounced signature of coastal upwelling, with higher concentrations nearshore in the central coast (36 – 40°N), and low concentrations in the Southern California Bight and in offshore waters (**Fig. 5b**). The signature of upwelling is also apparent in NPP (**Fig. 5c**), with high values near the coast, in particular in the central region, and decreasing values offshore. These patterns are consistent with observations, as discussed in prior work (Deutsch et al., 2021b)¶

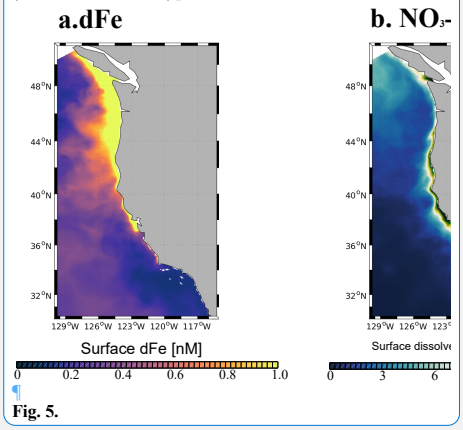

¶
Fig. 5.

the SBB come from limited sampling conducted quarterly as part of selected CalCOFI (California Cooperative Oceanic Fisheries Investigations) cruises (King and Barbeau, 2011). These samples mostly focus on the mixed layer and are too sparse in space and time to capture the effects of deep-water renewal events that ventilate the anoxic basins and allow uplifting and transport of deep waters towards the surface.

The agreement of the model dFe with observations (correlation coefficient $R=0.22$, $p<0.01$) is similar to that of other ocean biogeochemical models (Tagliabue et al., 2016). The model tends to underestimate the sharp dFe gradient between coastal and open ocean waters, overestimating dFe in the open ocean and producing too uniform concentrations offshore and at depth (**Fig. 4**). These biases are likely related to the simple Fe scavenging scheme, which assumes a constant Fe-binding ligand concentration of 0.6 nM. The small number and episodic nature of in-situ measurements may also explain some of the mismatches between model and observations.

At the scale of the CCS, the *High-flux* simulation produces lower surface dFe in the southern part of the domain (33°N to 36°N), and higher surface concentration in the northern part (40°N to 45°N) and near the central coast (**Fig. 5a**). While these patterns reflect a combination of internal Fe cycling and external inputs, the elevated dFe in the northern CCS, in particular offshore, can be partly attributed to higher aeolian deposition in that region (**Fig. S5)** as well as coastal inputs from the Juan De Fuca strait (Deutsch et al., 2021).

The model reproduces the typical signature of coastal upwelling, with higher concentrations of NO_3^- nearshore in the central coast (36°N-40°N) and low concentrations in the Southern California Bight and offshore (**Fig. 5b**). Similarly, the model reproduces high values of NPP near the coast, in particular along the central coast, and rapidly decreasing values offshore (**Fig. 5c**). Relative to previous modeling work (Deutsch et al., 2021) our simulations generate somewhat lower surface NO_3^- concentrations close to the coast, and sharper NPP gradients between the nearshore and offshore regions, which are consistent with the rapid decrease in primary productivity and chlorophyll shown by both satellite-based estimates and *in situ* data (Deutsch et al., 2021). These changes likely reflect the higher benthic Fe fluxes in our simulations (Equation 1), which increase phytoplankton productivity and promote nutrient drawdown near the coast.

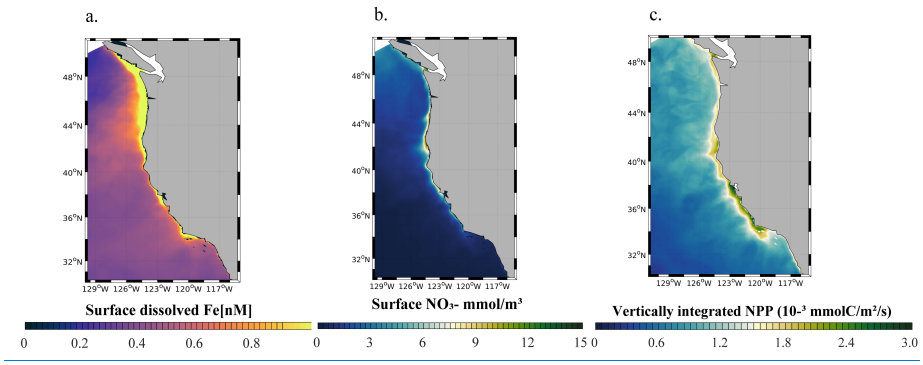

Fig. 5. (a) Surface dFe concentration, (b) surface NO_3^- concentration, and (c) vertically integrated net primary production (NPP) from the *High-flux* model simulation.

3.3 Hypoxia-off: Impact of benthic Fe flux from low-oxygen bottom water

We quantify the importance of benthic Fe fluxes from low-O_2 bottom waters in the Southern California Borderland by analyzing results from the *Hypoxia-off* experiment, in which we cap the high benthic Fe flux at a constant value (1.48 µmol m^{-2} d^{-1}) when O_2 declines below hypoxic conditions (65 mmol m^{-3}, see Section 2.5) **(Fig 6)**.

Deleted: (a),
Deleted: (b),
Formatted: Font: Not Bold
Deleted: (c)
Deleted: *Control*
Deleted: run
Deleted: **Low Oxygen Threshold**
Deleted: oxygen
Deleted: water
Deleted: *Low Oxygen Threshold* experiments
Deleted: oxygen
Deleted: a given threshold
Formatted: Subscript

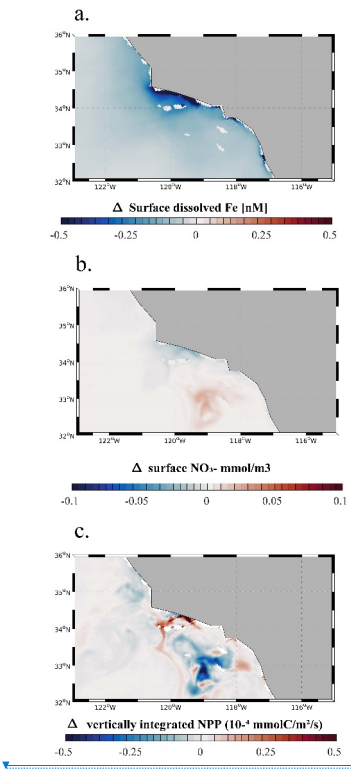

Figure 6. (a) Surface dFe anomalies, (b) Surface NO_3^- anomalies, and (c) vertically integrated net primary production (NPP) from the *Hypoxia-off* model run relative to the *High-flux* model run. The maps focus on the region around the SBB.

As expected, a decrease in benthic Fe flux from the anoxic basins in the *Hypoxia-off* simulation leads to a decrease in the surface dFe concentration (**Fig. 6a**). This decrease is particularly significant along the coast of the SBB, but also extends slightly into the open ocean (**Fig S6**). This trend indicates that dFe released from low-O_2 sediment is effectively transported to the surface and offshore, where it can affect primary production. The decrease in surface dFe caused by reduced benthic release causes a decline in NPP near the coast (**Fig. 6c**), where phytoplankton rely the most on benthic-derived Fe. NPP also shows a patchy increase in some regions,

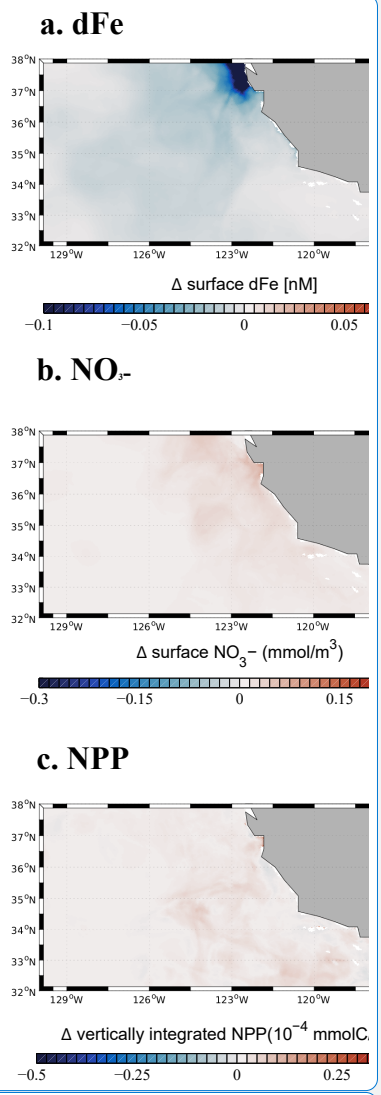

Deleted:

Deleted: ⁻ anomalies, and (c) vertically integrated net primary production (NPP) from the *Low Oxygen Threshold-100…ypoxia-off* model run relative to the *Control* ... [4]

Formatted: Font: Italic

Deleted: Graphs…he maps focus on areas ... [5]

Deleted: As expected, the forced decrease in benthic Fe flux in the *Low Oxygen Threshold-100* simulation leads to a significant decrease in the surface dFe concentration (**Fig. 6a**). This decrease is particularly strong along the coast, but also extends into the open ocean (**Fig S6**). This trend indicates that dFe released from low-oxygen sediment is effectively transported to the surface and offshore, where it can affect primary production. Consistently, the decrease in surface dFe drives a decline in NPP near the coast (**Fig.** ... [6]

Deleted:

especially between 32°N and 33°N and between 34°N and 35°N. This patchy increase can be explained by the relative importance of Fe vs. N limitation along a cross-shore productivity gradient. While near the SBB coast, phytoplankton is frequently Fe limited (up to 50% of the time in the model), especially following upwelling events, it tends to be almost exclusively N-limited moving offshore (Deutsch et al., 2021). This limitation pattern is consistent with observations from (King and Barbeau, 2011), who show that N:Fe ratios decrease moving from the coast to the open ocean (i.e., N is likely more limiting than Fe offshore). As Fe limitation reduces NPP near the coast in the *Hypoxia-off* experiment, NO_3^- utilization also declines, so that more NO_3^- can accumulate in surface waters (**Fig. 6b**). Shallow transport of excess NO_3^- in mesoscale eddies can further fertilize offshore waters (Damien et al., 2023), releasing local N limitation and fueling an increase in NPP (**Fig. 6c**).

3.4 Dust-off: Role of atmospheric Fe deposition

We evaluate the importance of aeolian Fe sources in the *Dust-off* simulation, in which atmospheric Fe deposition is set to zero. In this experiment, surface dFe decreases everywhere in the CCS, but the decrease is particularly evident in the open ocean and the northern part of the domain (**Fig. 7a**). This dFe decrease leads to a widespread reduction in NPP in the northern CCS (40°N to 48°N, **Fig. 7c**), with stronger negative anomalies away from the coast. The decline in NPP is accompanied by a broad decrease in NO_3^- utilization, particularly evident offshore, where phytoplankton rely mostly on Fe delivery by dust. In contrast, we observe a broad increase in NPP in the southern CCS (south of 40°S) and in coastal areas, likely reflecting increased availability of NO_3^- transported southward by the broad California Current. The response of NPP in coastal areas and the southern CCS, when the dust deposition of Fe is set to zero, demonstrates that phytoplankton in those regions relies mostly on benthic Fe fluxes, rather than dust deposition, as the main source of Fe.

Formatted: Font color: Text 1

Formatted: Left

Deleted: **8a…a**). This Fe…Fe decrease leads to a widespread decrease…eduction in NPP in the northern part of the domain (40N…CS (40°N to 48N, see…8°N, **Fig. S9…c**), with stronger negative anomalies away from the coast. The decline in NPP is accompanied by a broad decrease in NO_3^- utilization, particularly evident offshore, where phytoplankton rely mostly on Fe delivery by dust. In contrast, we observe a broad increase in NPP in the southern part of the domain…CS (south of 40°…S) and in coastal areas, reflecting increased availability of NO_3^- transported southward by the broad California Current. However, the relatively weak magnitude…he response of NPP responses to changes in …n coastal areas and the southern CCS, when the dust deposition demonstrate…f Fe is set to zero, demonstrates that phytoplankton in the coastal areas and the southern ... [7]

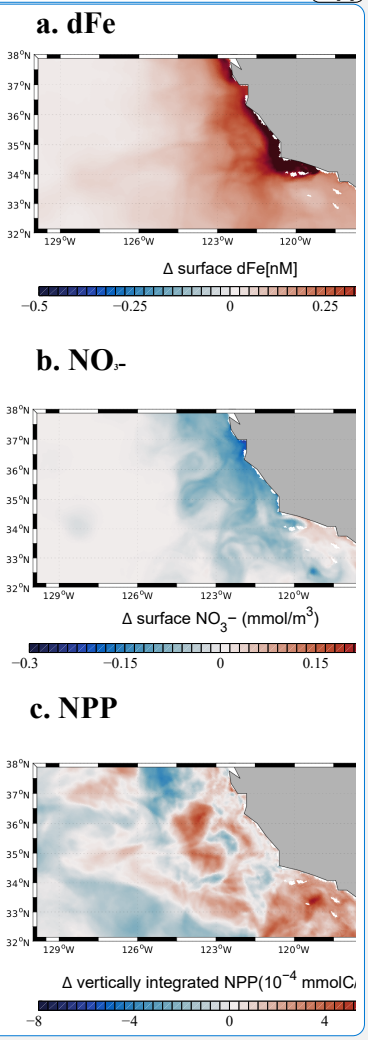

Deleted:

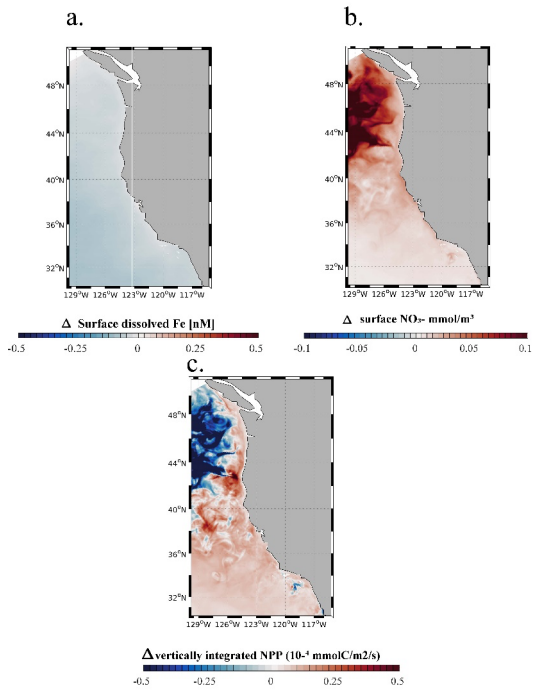

Figure 7. (a) Surface dissolved Fe, (b) surface NO_3^- anomalies, and (c) vertically integrated net primary production (NPP) from the *Dust-off* model run relative to the *High-flux* model run.

Deleted: Surface dFe anomalies

Deleted:),

Deleted: NO_3^- anomalies

Deleted:),

Deleted: anomalies (c) from the *High-flux* model run relative to the *Control* model run. The graphs focus on areas around the SBB. For the full model domain of the U.S West coast see **Fig. S8**.¶

¶

... [8]

Deleted: *Control* model run. The graphs focus on the areas around the SBB. For the full model domain of the U.S West coast see **Fig. S9**.

4. Discussion

4.1 Benthic Fe flux feedbacks on SBB biogeochemistry

The influence of bottom water O_2 concentration on the exchange of solutes between the sediment and the water column has been well documented (Soetaert et al., 2000; Sommer et al., 2016; Testa et al., 2013). Under hypoxic or anoxic bottom water conditions, organic matter sedimentation sustains anaerobic respiration at the sediment-water interface and in the sediment (Furrer and Wehrli, 1993; Middelburg and Levin, 2009a). Reduced compounds accumulate in pore waters forming chemical gradients (Widdows and Brinsley, 2002) that result in the flux of solutes such as Fe(II) out of the sediment, and their accumulation in bottom water (Jørgensen and Nelson, 2004; McMahon and Chapelle, 1991; Middelburg and Levin, 2009b; Yao et al., 2016). Similar conditions are observed in the SBB, where high sedimentation rates, water column denitrification below the sill depth, and high pore-water concentrations of sulfide and Fe(II) have been observed (Behl and Kennett, 1996; Bray et al., 1999; Goericke et al., 2015; Sholkovitz and Soutar, 1975; Sigman et al., 2003; White et al., 2019).

Deleted: The influence of bottom water oxygen concentration on the exchange of solutes between the sediment and the water column has been well documented (Soetaert et al., 2000; Sommer et al., 2016; Testa et al., 2013). Under hypoxic or anoxic bottom water conditions, organic matter sedimentation sustains anerobic respiration at the sediment-water interface and in the sediment (Furrer and Wehrli, 1993; Middelburg and Levin, 2009). Reduced compounds accumulate in pore waters forming chemical gradients (Widdows and Brinsley, 2002) that result in the flux of solutes such as Fe(II) out of the sediment, and their accumulation in bottom water (Jørgensen and Nelson, 2004; McMahon and Chapelle, 1991; Middelburg and Levin, 2009; Yao et al., 2016). Similar conditions are observed in the SBB, where high sedimentation rates, water column denitrification below the sill depth, and high pore-water concentrations of sulfide and Fe(II) have been observed (Behl and Kennett, 1996; Bray et al., 1999; Goericke et al., 2015; Sholkovitz and Soutar, 1975; Sigman et al., 2003; White et al., 2019).¶

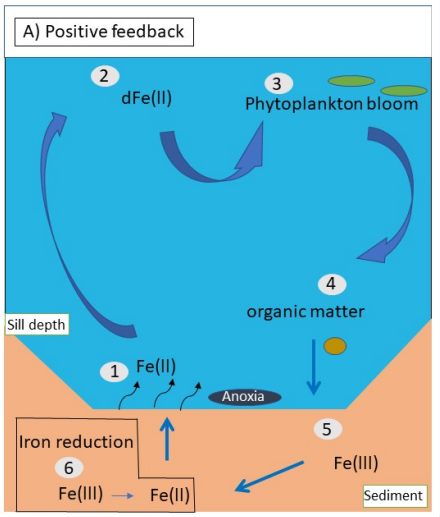

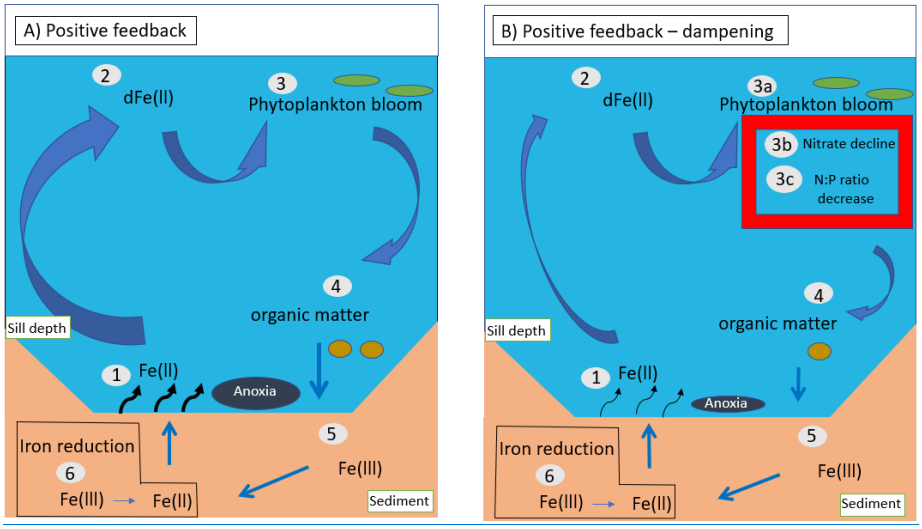

Figure 8. Schematic illustrating feedback loops between benthic Fe release, nutrient cycles, and productivity in the Santa Barbara Basin. (a) Positive feedback loop: 1. Benthic Fe is released into the oxygen-poor bottom water. 2. Upwelled Fe reaches the surface ocean increasing dissolved Fe concentrations. 3. Dissolved Fe is assimilated by phytoplankton, fueling blooms and production of organic matter and siderophores, i.e., ligands used to chelate ferric iron. 4. Organic matter is exported from the surface to the deep ocean. 5. Organic matter accumulates at the sediment-water interface. 6. During remineralization, iron-reducing bacteria reduce Fe(III) to Fe(II), increasing benthic dFe release. (b) Positive feedback loop – dampening : 1-3 (not including 3b and 3c) and 4-6 are identical to (a). Parts 3b and 3c illustrate the decline of NO_3^- at the surface caused by the reduction in Fe limitation, which together with increased denitrification in anoxic waters and sediment would limit the potential increase in primary production and export from the surface caused by Fe fertilization. Together with enhanced release of phosphate from anoxic sediment, a reduction in the available NO_3^- could also reduce the N:P ratio of phytoplankton. Ultimately, the effect of a decrease of NO_3^- on export and remineralization of organic matter would limit the increase of benthic Fe(II) fluxes, dampening the positive feedback.

Deleted: 9.

Deleted: in the SBB (A):

Deleted: release

Deleted: anoxic (<3 µM), or severely hypoxic (3-20 µM)

Deleted:

Deleted: contributing to dFe. 3.

Deleted: producing phytoplankton

Deleted: ,

Deleted: at the surface.

Deleted: of organic matter

Deleted:). Negative

Formatted: Subscript

Formatted: Superscript

Formatted: Subscript

Formatted: Superscript

Formatted: Subscript

Formatted: Superscript

Deleted: (b) Positive feedback loop in the SBB (B): – dampening : 1-3 (not including 3 b3b and c3c) and 4-6 are identical to (A). Parta). Parts 3b and 3c showsillustrate the decline of NO_3^- at the surface caused by the release of Fe limitation, which together with fixed-N loss in anoxic sediment would limit the increase in primary production and export production. Together with enhanced release of phosphate from the amplification of dFe, which causes a decrease inanoxic sediment, this could also reduce the N:P ratio of phytoplankton. Ultimately, these processes inhibit a further increase of the benthic Fe(II) release, dampening the positive feedback.

The intense flux of dFe from the sediment suggests the potential for biogeochemical feedbacks in the SBB and more broadly in the CCS (as shown by Figs. 5 – 7). Under a positive feedback scenario (illustrated in Fig. 8a), anoxic and nearly anoxic bottom water conditions facilitate Fe(II) diffusion from the sediment into the bottom water. In the SBB, this Fe eventually reaches the surface via upwelling and mixing processes, which are likely enhanced in the presence of complex bathymetry and islands in the Southern California Bight (Kessouri et al., 2020). This additional dFe input fertilizes coastal waters and increases primary production. Newly formed organic matter eventually sinks towards the seafloor as a rain of organic particles, supporting low-oxygen concentrations in the bottom water, and fueling anaerobic respiration, including Fe reduction, in the sediment. This chain of processes thus represents a positive feedback loop that maintains high Fe(II) release from the sediment, as long as the bottom water remains hypoxic or anoxic (Mills et al., 2004; Noffke et al., 2012; Sañudo-Wilhelmy et al., 2001; Dale et al., 2015; Wallmann et al., 2022).

Our simulations also indicate the potential for complex biogeochemical responses between Fe, NO_3^- and NPP, which could limit the effects of these feedbacks. Specifically, the positive feedback loop is damped in our conceptual model by increased NO_3^- limitation and elevated N-loss in anoxic sediments under oxygen-deficient bottom waters at higher Fe supply (illustrated by Fig. 8b), which would in turn limit the increase in NPP. Transport of N-depleted coastal waters can further reduce NPP offshore, counteracting the positive feedback. In addition, the positive feedback would be also damped by Fe scavenging, which is magnified at high dissolved Fe concentrations, unless Fe-binding ligands also increase. This damping effect is particularly strong in our model, where a constant ligand concentration of 0.6 nM is used, above which scavenging rapidly increases (Section 2). Such a negative feedback between scavenging and benthic Fe fluxes is consistent with the global modeling study by Somes et al. (2021).

Additional processes may further modulate these feedback loops. Increased anoxia in bottom water and sediment favors the removal of fixed N by denitrification (Goericke et al., 2015; White et al., 2019). Upwelling of NO_3^--depleted waters would then reduce surface productivity by increasing N limitation (Gruber and Deutsch, 2014). Release of Fe(II) from the sediment could also impact phosphate dynamics. Phosphate is scavenged by Fe during oxidation of Fe(II) in the water column

Deleted: The intense flux of dFe from the sediment suggests the potential for positive biogeochemical feedbacks in the SBB and more broadly in the CCS (**Figs. 6 – 8**). However, our simulations also indicate the presence of complex biogeochemical responses between Fe, NO_3^- and NPP that may dampen the effects of these feedbacks.¶
Under a positive feedback scenario (**Fig. 9a**), anoxic and nearly anoxic bottom water conditions facilitate Fe(II) diffusion from the sediment into the bottom water. In the SBB, this Fe eventually reaches the surface via upwelling and mixing processes, which are likely enhanced in the presence of complex bathymetry and islands (Kessouri et al., 2020). This additional dFe input fertilizes coastal waters and increases primary production. Newly formed organic matter eventually sinks towards the seafloor as a rain of organic particles, supporting low-oxygen concentrations in the bottom water, and fueling anaerobic respiration, including Fe reduction, in the sediment. This chain of processes thus represents a positive feedback loop that maintains high Fe(II) release from the sediment, as long as the bottom water remains hypoxic or anoxic (Mills et al., 2004; Noffke et al., 2012; Sañudo-Wilhelmy et al., 2001; Dale et al., 2015). However, our simulations suggest that this positive feedback loop is dampened by increased NO_3^- limitation under higher Fe supply (**Fig. 9b**), which would limit the increase in NPP. Transport of N-depleted coastal waters reduces NPP offshore (**Fig. 7**), further counteracting the positive feedback loop.¶
Additional processes may dampen or alter this feedback loop. Increased anoxia in bottom water and sediment favors the removal of fixed N by denitrification (Goericke et al., 2015; White et al., 2019). Upwelling of NO_3^--depleted waters would then reduce surface productivity by increasing N limitation (Gruber and Deutsch, 2014). Release of Fe(II) from the sediment could also impact phosphate dynamics in the SBB. Phosphate is scavenged by iron during oxidation of Fe(II) in the water column and sediment because of the ability of Fe(III) minerals to bind phosphate. After burial, phosphate is released due to reduction of solid Fe(III) minerals to dissolved Fe(II), and diffuses upward to be either re-adsorbed by Fe(III) at the oxic sediment-water interface, or released to the bottom water under anoxic conditions (Dijkstra et al., 2014). The latter scenario is consistent with our in-situ benthic flux chamber measurements revealing increased phosphate releases from the sediment with increased SBB depth (data not shown). Increased release of phosphate into the water column, and transport to the surface, could decreases the N:P ratio of phytoplankton, especially downstream of waters where denitrification occurred (Deutsch et al., 2007). In the presence of N limitation, these conditions could favor the activity of nitrogen-fixing microorganisms (Mills et al., 2004; Noffke et al., 2012; Sañudo-Wilhelmy et al., 2001), further modulating surface NPP (Deutsch et al., 2007).¶
4.2 Contribution of physical transport on surface Fe¶
Our numerical experiments suggest that Fe released into the deep SBB can reach and fertilize surface waters. This finding highlights the critical role of bottom water upwelling and mixing in the SBB. There is ample literature describing seasonal surface circulation and bottom water renewal and its effect on nutrients in the SBB (Bray et al., 1999; Hendershott and Winant, 1996; Sholkovitz and Gieskes, 1971). However, the frequency and rate of seasonal bottom water flushin ... [9]

and sediment because of the ability of Fe(III) minerals to bind it. After burial, phosphate is released due to reduction of solid Fe(III) minerals to dissolved Fe(II), and diffuses upward to be either re-adsorbed by Fe(III) at the oxic sediment-water interface, or released to the bottom water under anoxic conditions (Dijkstra et al., 2014). The latter scenario is consistent with our in-situ benthic flux chamber measurements revealing increased phosphate release from the sediment with increased depth in the SBB (Yousavich et al., 2023). Higher release of phosphate into the water column, and transport to the surface, could decrease the N:P ratio of phytoplankton, especially downstream of waters where denitrification occurred (Deutsch et al., 2007). In the presence of N limitation, these conditions could favor the activity of nitrogen-fixing microorganisms (Mills et al., 2004; Noffke et al., 2012; Sañudo-Wilhelmy et al., 2001), which could further modulate surface NPP (Deutsch et al., 2007).

4.2 Contribution of physical transport on surface Fe

Our numerical experiments suggest that Fe released into the deep SBB can reach surface waters and fertilize them. This finding highlights the critical role of bottom water upwelling and mixing in the deep basins of the Southern California Borderland. There is ample literature describing seasonal surface circulation and bottom water renewal and their effect on nutrients in the SBB (Bray et al., 1999; Hendershott and Winant, 1996; Sholkovitz and Gieskes, 1971). However, the frequency and rate of seasonal bottom water flushing events, and the processes responsible for vertical mixing and upwelling across hundreds of meters remain poorly understood (Shiller et al., 1985; Sholkovitz and Gieskes, 1971; White et al., 2019). It is likely that interaction between wind-driven upwelling events and submesoscale eddies, which are particularly intense inside the Santa Barbara Channel (Kessouri et al., 2020), favors upward mixing of deep bottom water in the wake of flushing events, connecting deep bottom waters to the surface.

4.3 Quantifying expansion of anoxia in the SBB

Changes in source waters and global O_2 loss have contributed to decreasing O_2 levels throughout the Southern California Bight and the SBB (Zhou et al., 2022). With the outlook of a continuing decline in oceanic O_2 (Bopp et al., 2013; Kwiatkowski et al., 2020), quantifying the expansion of hypoxic and anoxic zones in the SBB is vital to understand the dynamics and fate of Fe(II) and other reduced compounds, such as ammonium and hydrogen sulfide, in deep low-oxygen waters.

Deleted:

Deleted: Changes in source waters and global oxygen loss in the Southern California Bight have contributed to decreasing O_2 levels throughout the Southern California Bight and the SBB (Zhou et al., 2022). With the outlook of a continuing decline in oceanic oxygen (Bopp et al., 2013; Kwiatkowski et al., 2020), quantifying the expansion of hypoxic and anoxic zones in the SBB is vital to understand the dynamics and fate of Fe(II) and other reduced compounds (e.g., ammonium (NH_4^+), hydrogen sulfide (H_2S)) in deep low-oxygen waters. In the SBB, bottom water renewal events have experienced a decline in frequency and magnitude, driving an expansion of hypoxic and anoxic conditions in deep waters (White et al., 2019). This expansion leads to an increase in anaerobic reactions, such as denitrification in the water column (White et al., 2019) as well as Fe reduction, sulfate reduction, and dissimilatory nitrate reduction to ammonium (DNRA) in the sediment (Valentine et al., 2016; Treude et al., 2021; Sommer et al., 2016). Expansion of low oxygen waters could intensify the positive feedback loop between Fe release, NPP and O_2 loss (**Fig. 9**). However, to date, despite the evidence for more frequent anoxia, there is no clear quantitative record of the vertical or horizontal expansions of oxygen-deficient waters in the SBB.

Page Break

¶

5. Conclusion¶

Our field campaign in the SBB measured a remarkably high flux of Fe(II) from the sediment (0.23 – 4.9 mmol m^{-2} d^{-1}), greater than in previous studies from this region (Severmann et al., 2010) and from other oxygen minimum zones (Dale et al. 2015; Homoky et al. 2021). Using a series of simulations with an ocean biogeochemical model, we show that this high Fe release from deep, low-oxygen sediment has a significant impact on surface nutrients and productivity in the SBB and the Southern California Bight, where Fe is often limiting (Hogle et al., 2018). We also highlight the impacts of coastal Fe inputs on waters further offshore. While phytoplankton in coastal areas directly benefit from Fe fertilization, increased NO_3^- utilization in coastal waters can cause N-limitation of phytoplankton further downstream in open-ocean areas. Thus, benthic Fe fluxes can modulate Fe and NO_3^- limitation in ways that partially counteract one another along the cross-shore productivity gradient of the CCS. Our model simulations also suggest that Fe inputs from atmospheric deposition are mostly important in the open ocean north of 40°N, where phytoplankton rely on Fe delivery by dust. However, we also show that changes in atmospheric Fe deposition can alter ocean productivity in the southern CCS by altering NO_3^- utilization further downstream. Our results support the idea that benthic Fe fluxes are the major source of Fe in the southern CCS and are supplemented by atmospheric deposition in the northwestern region, leading to relatively high NPP coastwide.¶

Over the entire U.S. West Coast, changes in the dependence of benthic Fe release on bottom O_2 can halve (*Low Oxygen Threshold-100*) or double (*High-flux*) the mean benthic Fe flux. While our observations are based on snapshots of O_2 and Fe flux, they have implications for the temporal variability of Fe supply. High benthic Fe fluxes are observed during the anoxic fall season, while seasonal flushing [...] [10]

In the SBB, bottom water renewal events have experienced a decline in frequency and magnitude, driving an expansion of hypoxic and anoxic conditions in deep waters (White et al., 2019). This expansion has led to an increase in anaerobic reactions, such as denitrification in the water column (White et al., 2019) as well as sulfur cycling in the sediment (Valentine et al., 2016). Expansion of low O_2 waters could intensify the positive feedback loop between Fe release, NPP and O_2 loss (**Fig. 8**). However, to date, despite growing evidence for more frequent anoxia, there is no clear quantitative record of the vertical or horizontal expansions of oxygen-deficient waters in the SBB.

Deleted: Fe reduction, sulfate reduction, and dissimilatory nitrate reduction to ammonium (DNRA)

Deleted: (Valentine et al., 2016; Treude et al., 2021; Sommer et al., 2016)

5. Conclusion

Our field campaign in the SBB measured a remarkably high flux of Fe(II) from the sediment (0.23 – 4.9 mmol m^{-2} d^{-1}), greater than in previous studies from this region (Severmann et al., 2010) and from other oxygen minimum zones (Dale et al. 2015; Homoky et al. 2021). While these observations are based on snapshots of O_2 and Fe fluxes, they have implications for the temporal variability of Fe supply. High benthic Fe fluxes are observed during the anoxic fall season, while seasonal flushing in winter and spring likely decreases them by increasing bottom water O_2 and Fe oxidation and retention near the sediment.

Using a series of simulations with an ocean biogeochemical model, we show that this high Fe release from deep, low-oxygen sediment can reach the surface and impact nutrients and productivity in the SBB and the Southern California Bight, where Fe is often limiting (Hogle et al., 2018). We also highlight the impacts of coastal Fe inputs on waters further offshore. While phytoplankton in coastal areas directly benefits from Fe fertilization, increased NO_3^- utilization in coastal waters can increase N-limitation of phytoplankton further downstream in open-ocean areas. Thus, benthic Fe fluxes can modulate Fe and NO_3^- limitation in ways that partially counteract one another along the cross-shore productivity gradient of the CCS. Our simulations also suggest that Fe inputs from atmospheric deposition are mostly important in the open ocean north of 40°N, where phytoplankton rely on Fe delivery by dust. However, we also show that changes in atmospheric Fe deposition can affect ocean productivity in the southern CCS by altering NO_3^- utilization further downstream. Our results support the idea that benthic Fe fluxes are the major source of Fe in the southern CCS and are supplemented by atmospheric deposition in northwestern and offshore waters, leading to relatively high NPP coastwide.

We suggest that benthic Fe fluxes from deep anoxic basins reach the surface in the SBB, contributing to feedbacks between Fe and NO_3^- limitation and NPP. Specifically, high Fe fluxes from low-oxygen sediment support higher NPP near the coast, in turn leading to increased respiration and O_2 loss at depth, maintaining high Fe release. This positive feedback is damped by increased NO_3^- limitation, which reduces NPP downstream of coastal regions. This benthic-pelagic coupling demonstrates the importance of sediment-derived Fe fluxes on the coastal ecosystem of the CCS, and the role of vertical transport processes in connecting deep environments to surface

Deleted: ocean

Deleted: loop

Deleted: dampened

waters along continental margins. Our results are thus consistent with previous work from the Peruvian coastal upwelling (Wallmann et al., 2022), suggesting that oceanic O_2 loss could drive an increase in benthic Fe fluxes, enhancing local productivity and leading to further O_2 loss. This positive feedback could be stabilized by loss of fixed nitrogen under expanded anaerobic conditions.

It is likely that feedbacks of the type highlighted by (Wallmann et al., 2022) and our work in the SBB are at play more broadly along low-oxygen upwelling systems and coastal OMZ. Further studies should focus on the coupling between benthic processes and Fe and nutrient cycling in these regions. For example, fixed nitrogen loss by denitrification and enhanced release of phosphorous under low-oxygen bottom water are likely to further modulate these interactions. Seasonal studies based on stable isotope, radiotracer, and geochemical techniques are required to track the fate and transport of nutrients in low-O_2 coastal regions, clarifying the dynamics and sensitivities of the underlying microbial metabolisms. Ocean biogeochemical models for regional and global studies should incorporate new observations of benthic fluxes and their sensitivity to bottom O_2 and other environmental variables. This would expand the ability of models to better capture the effects of long-term oceanic O_2 loss, and the feedbacks between benthic nutrient fluxes and surface productivity.

Deleted: We highlight the need for further studies focusing on feedbacks between benthic processes and surface biogeochemistry. For example, fixed N

Formatted: Justified, Space Before: 12 pt, After: 12 pt, Line spacing: 1.5 lines

Deleted: the SBB and similar

Deleted: shedding light on

Deleted: that influences these dynamics

Deleted: model adaptation

Deleted: shed light on

Deleted: impact

Deleted: O_2 variability, from seasonal

Deleted: interannual and longer timescales, including

Deleted: on

Deleted: biogeochemistry.¶

Acknowledgements

We thank the captain and crew of R/V Atlantis, the crew of ROV Jason, the crew of AUV Sentry, and the science party of research cruise AT42-19 for their technical and logistical support. We thank Q. Qin, M. O'Beirne, A. Mazariegos, X. Moreno, and A. Eastman for assisting with shipboard analyses. Funding for this work was provided by the US National Science Foundation, NSF OCE-1829981 (to TT), OCE-1756947 and OCE-1830033 (to DLV), and OCE-2023493 (to DB and ALP). Computational resources were provided by the Expanse system at the San Diego Supercomputer Center through allocation TG-OCE170017 from the Extreme Science and Engineering Discovery Environment (XSEDE), which was supported by National Science Foundation grant 1548562.

Code availability

The physical and biogeochemical codes used for our simulations can be accessed at: https://github.com/UCLA-ROMS/Code.

The model output can be accessed through Zenodo: (link will be provided before publication)

Formatted: Font color: Red

Data availability

In-situ benthic Fe flux data are accessible through the Biological & Chemical Oceanography Data Management Office (BCO-DMO) under the following DOI: 10.26008/1912/bco-dmo.896706.1.

Deleted: (link will be provided before publication).

Author contributions.

DR, TT, DB, and AP conceived this study. DM, DJY, FJ, FW, ECA, KMG, DLV and TT conducted the sampling at sea. DJY transformed and interpreted ROV Jason data. FJ and FW constructed and managed benthic flux chambers. DYJ and DR analyzed Fe(II) and assisted with the flux calculation. MM provided the compiled Fe measurements along the U.S. West Coast. AP and MS performed the model simulations. DR, DB, AP and TT wrote the manuscript with input from all co-authors.

Competing interests

Some authors are members of the editorial board of Biogeosciences. The peer-review process was guided by an independent editor, and the authors have no other competing interests to declare.

Deleted: The

Deleted: declare that they

Formatted: Space Before: 12 pt, After: 12 pt

Deleted: known

Deleted: financial

Deleted: or personal relationships that could have appeared

Deleted: influence the work reported in this paper

References

Aumont, O., Ethé, C., Tagliabue, A., Bopp, L., and Gehlen, M.: PISCES-v2: An ocean biogeochemical model for carbon and ecosystem studies, Geosci. Model Dev., 8, 2465–2513, https://doi.org/10.5194/gmd-8-2465-2015, 2015.

Behl, R. J. and Kennett, J. P.: Brief interstadial events in the Santa Barbara basin, NE Pacific, during the past 60 kyr, Nature, 379, 243–246, https://doi.org/10.1038/379243a0, 1996.

Biller, D. V. and Bruland, K. W.: Sources and distributions of Mn, Fe, Co, Ni, Cu, Zn, and Cd relative to macronutrients along the central California coast during the spring and summer upwelling season, Mar. Chem., 155, 50–70, https://doi.org/10.1016/j.marchem.2013.06.003, 2013.

Boiteau, R. M., Till, C. P., Coale, T. H., Fitzsimmons, J. N., Bruland, K. W., and Repeta, D. J.: Patterns of iron and siderophore distributions across the California Current System, Limnol. Oceanogr., 64, 376–389, https://doi.org/10.1002/lno.11046, 2019.

Bopp, L., Resplandy, L., Orr, J. C., Doney, S. C., Dunne, J. P., Gehlen, M., Halloran, P., Heinze, C., Ilyina, T., Séférian, R., Tjiputra, J., and Vichi, M.: Multiple stressors of ocean ecosystems in the 21st century: projections with CMIP5 models, Biogeosciences, 10, 6225–6245, https://doi.org/10.5194/bg-10-6225-2013, 2013.

Brander, K., Cochrane, K., Barange, M., and Soto, D.: Climate Change Implications for Fisheries and Aquaculture, in: Climate Change Impacts on Fisheries and Aquaculture, edited by: Phillips, B. F. and Pérez-Ramírez, M., John Wiley & Sons, Ltd, Chichester, UK, 45–62, https://doi.org/10.1002/9781119154051.ch3, 2017.

Bray, N. A., Keyes, A., and Morawitz, W. M. L.: The California Current system in the Southern California Bight and the Santa Barbara Channel, J. Geophys. Res. Oceans, 104, 7695–7714, https://doi.org/10.1029/1998JC900038, 1999.

Bruland, K. W., Rue, E. L., and Smith, G. J.: Iron and macronutrients in California coastal upwelling regimes: Implications for diatom blooms, Limnol. Oceanogr., 46, 1661–1674, https://doi.org/10.4319/lo.2001.46.7.1661, 2001.

Bruland, K. W., Middag, R., and Lohan, M. C.: Controls of Trace Metals in Seawater, in: Treatise on Geochemistry, Elsevier, 19–51, https://doi.org/10.1016/B978-0-08-095975-7.00602-1, 2014.

Bundy, R. M., Biller, D. V., Buck, K. N., Bruland, K. W., and Barbeau, K. A.: Distinct pools of dissolved iron-binding ligands in the surface and benthic boundary layer of the California Current, Limnol. Oceanogr., 59, 769–787, https://doi.org/10.4319/lo.2014.59.3.0769, 2014.

Bundy, R. M., Abdulla, H. A. N., Hatcher, P. G., Biller, D. V., Buck, K. N., and Barbeau, K. A.: Iron-binding ligands and humic substances in the San Francisco Bay estuary and estuarine-

influenced shelf regions of coastal California, Mar. Chem., 173, 183–194, https://doi.org/10.1016/j.marchem.2014.11.005, 2015.

Bundy, R. M., Jiang, M., Carter, M., and Barbeau, K. A.: Iron-Binding Ligands in the Southern California Current System: Mechanistic Studies, Front. Mar. Sci., 3, https://doi.org/10.3389/fmars.2016.00027, 2016.

Capet, X., Campos, E. J., and Paiva, A. M.: Submesoscale activity over the Argentinian shelf, Geophys. Res. Lett., 35, https://doi.org/10.1029/2008GL034736, 2008.

Carr, M.-E. and Kearns, E. J.: Production regimes in four Eastern Boundary Current systems, Deep Sea Res. Part II Top. Stud. Oceanogr., 50, 3199–3221, https://doi.org/10.1016/j.dsr2.2003.07.015, 2003.

Chappell, P., Armbrust, E., Barbeau, K., Bundy, R., Moffett, J., Vedamati, J., and Jenkins, B.: Patterns of diatom diversity correlate with dissolved trace metal concentrations and longitudinal position in the northeast Pacific coastal-offshore transition zone, Mar. Ecol. Prog. Ser., 609, 69–86, https://doi.org/10.3354/meps12810, 2019.

Chase, Z.: Iron, nutrient, and phytoplankton distributions in Oregon coastal waters, J. Geophys. Res., 107, 3174, https://doi.org/10.1029/2001JC000987, 2002.

Chase, Z., Johnson, K. S., Elrod, V. A., Plant, J. N., Fitzwater, S. E., Pickell, L., and Sakamoto, C. M.: Manganese and iron distributions off central California influenced by upwelling and shelf width, Mar. Chem., 95, 235–254, https://doi.org/10.1016/j.marchem.2004.09.006, 2005.

Chavez, F. P. and Messié, M.: A comparison of Eastern Boundary Upwelling Ecosystems, Prog. Oceanogr., 83, 80–96, https://doi.org/10.1016/j.pocean.2009.07.032, 2009.

Dale, A. W., Nickelsen, L., Scholz, F., Hensen, C., Oschlies, A., and Wallmann, K.: A revised global estimate of dissolved iron fluxes from marine sediments: GLOBAL BENTHIC IRON FLUXES, Glob. Biogeochem. Cycles, 29, 691–707, https://doi.org/10.1002/2014GB005017, 2015.

Damien, P., Bianchi, D., McWilliams, J. C., Kessouri, F., Deutsch, C., Chen, R., and Renault, L.: Enhanced Biogeochemical Cycling Along the U.S. West Coast Shelf, Glob. Biogeochem. Cycles, 37, e2022GB007572, https://doi.org/10.1029/2022GB007572, 2023.

Deutsch, C., Sarmiento, J. L., Sigman, D. M., Gruber, N., and Dunne, J. P.: Spatial coupling of nitrogen inputs and losses in the ocean, Nature, 445, 163–167, https://doi.org/10.1038/nature05392, 2007.

Deutsch, C., Brix, H., Ito, T., Frenzel, H., and Thompson, L.: Climate-Forced Variability of Ocean Hypoxia, Science, 333, 336–339, https://doi.org/10.1126/science.1202422, 2011.

Deutsch, C., Frenzel, H., McWilliams, J. C., Renault, L., Kessouri, F., Howard, E., Liang, J.-H., Bianchi, D., and Yang, S.: Biogeochemical variability in the California Current System, Prog. Oceanogr., 196, 102565, https://doi.org/10.1016/j.pocean.2021.102565, 2021.

Deleted: 2021a

Dijkstra, N., Kraal, P., Kuypers, M. M. M., Schnetger, B., and Slomp, C. P.: Are Iron-Phosphate Minerals a Sink for Phosphorus in Anoxic Black Sea Sediments?, PLOS ONE, 9, e101139, https://doi.org/10.1371/journal.pone.0101139, 2014.

Evans, N., Schroeder, I. D., Pozo Buil, M., Jacox, M. G., and Bograd, S. J.: Drivers of Subsurface Deoxygenation in the Southern California Current System, Geophys. Res. Lett., 47, https://doi.org/10.1029/2020GL089274, 2020.

Firme, G. F., Rue, E. L., Weeks, D. A., Bruland, K. W., and Hutchins, D. A.: Spatial and temporal variability in phytoplankton iron limitation along the California coast and consequences for Si, N, and C biogeochemistry: SPATIAL AND TEMPORAL VARIABILITY IN PHYTOPLANKTON IRON, Glob. Biogeochem. Cycles, 17, https://doi.org/10.1029/2001GB001824, 2003.

Furrer, G. and Wehrli, B.: Biogeochemical processes at the sediment-water interface: measurements and modeling, Appl. Geochem., 8, 117–119, https://doi.org/10.1016/S0883-2927(09)80021-8, 1993.

García-Reyes, M. and Largier, J.: Observations of increased wind-driven coastal upwelling off central California, J. Geophys. Res., 115, C04011, https://doi.org/10.1029/2009JC005576, 2010.

Goericke, R., Bograd, S. J., and Grundle, D. S.: Denitrification and flushing of the Santa Barbara Basin bottom waters, Deep Sea Res. Part II Top. Stud. Oceanogr., 112, 53–60, https://doi.org/10.1016/j.dsr2.2014.07.012, 2015.

Grasshoff, K., and Ehrhardt, M.: Methods of seawater analysis, 3rd, completely rev. and extended ed. ed., Wiley-VCH, Weinheim, New York, xxxii, 600 pp., 1999.

Hawco, N. J., Barone, B., Church, M. J., Babcock-Adams, L., Repeta, D. J., Wear, E. K., Foreman, R. K., Björkman, K. M., Bent, S., Van Mooy, B. A. S., Sheyn, U., DeLong, E. F., Acker, M., Kelly, R. L., Nelson, A., Ranieri, J., Clemente, T. M., Karl, D. M., and John, S. G.: Iron Depletion in the Deep Chlorophyll Maximum: Mesoscale Eddies as Natural Iron Fertilization Experiments, Glob. Biogeochem. Cycles, 35, https://doi.org/10.1029/2021GB007112, 2021.

Hendershott and Winant: Surface Circulation in the Santa Barbara Channel, Oceanography, 9, 114–121, https://doi.org/10.5670/oceanog.1996.14, 1996.

Hogle, S. L., Dupont, C. L., Hopkinson, B. M., King, A. L., Buck, K. N., Roe, K. L., Stuart, R. K., Allen, A. E., Mann, E. L., Johnson, Z. I., and Barbeau, K. A.: Pervasive iron limitation at subsurface chlorophyll maxima of the California Current, Proc. Natl. Acad. Sci., 115, 13300–13305, https://doi.org/10.1073/pnas.1813192115, 2018.

Homoky, W. B., Conway, T. M., John, S. G., König, D., Deng, F., Tagliabue, A., and Mills, R. A.: Iron colloids dominate sedimentary supply to the ocean interior, Proc. Natl. Acad. Sci., 118, e2016078118, https://doi.org/10.1073/pnas.2016078118, 2021.

Deleted: Deutsch, C., Frenzel, H., McWilliams, J. C., Renault, L., Kessouri, F., Howard, E., Liang, J.-H., Bianchi, D., and Yang, S.: Biogeochemical variability in the California Current System, Prog. Oceanogr., 196, 102565, https://doi.org/10.1016/j.pocean.2021.102565, 2021b.¶

Deleted: ., Kremlingl, K.,

Deleted: Seawater Analysis

Deleted: Edn.,

Deleted: Wiley–VCH,

Deleted:

John, S. G., Mendez, J., Moffett, J., and Adkins, J.: The flux of iron and iron isotopes from San Pedro Basin sediments, Geochim. Cosmochim. Acta, 93, 14–29, https://doi.org/10.1016/j.gca.2012.06.003, 2012.

Johnson, K. S., Elrod, V. A., Fitzwater, S. E., Plant, J. N., Chavez, F. P., Tanner, S. J., Gordon, R. M., Westphal, D. L., Perry, K. D., Wu, J., and Karl, D. M.: Surface ocean-lower atmosphere interactions in the Northeast Pacific Ocean Gyre: Aerosols, iron, and the ecosystem response, Glob. Biogeochem. Cycles, 17, https://doi.org/10.1029/2002GB002004, 2003.

Jørgensen, B. B. and Nelson, D. C.: Sulfide oxidation in marine sediments: Geochemistry meets microbiology, in: Sulfur Biogeochemistry - Past and Present, Geological Society of America, https://doi.org/10.1130/0-8137-2379-5.63, 2004.

Kessouri, F., Bianchi, D., Renault, L., McWilliams, J. C., Frenzel, H., and Deutsch, C. A.: Submesoscale Currents Modulate the Seasonal Cycle of Nutrients and Productivity in the California Current System, Glob. Biogeochem. Cycles, 34, e2020GB006578, https://doi.org/10.1029/2020GB006578, 2020.

King, A. L. and Barbeau, K. A.: Dissolved iron and macronutrient distributions in the southern California Current System, J. Geophys. Res., 116, C03018, https://doi.org/10.1029/2010JC006324, 2011.

Kononets, M., Tengberg, A., Nilsson, M., Ekeroth, N., Hylén, A., Robertson, E. K., van de Velde, S., Bonaglia, S., Rütting, T., Blomqvist, S., and Hall, P. O. J.: In situ incubations with the Gothenburg benthic chamber landers: Applications and quality control, J. Mar. Syst., 214, 103475, https://doi.org/10.1016/j.jmarsys.2020.103475, 2021.

Kwiatkowski, L., Torres, O., Bopp, L., Aumont, O., Chamberlain, M., Christian, J. R., Dunne, J. P., Gehlen, M., Ilyina, T., John, J. G., Lenton, A., Li, H., Lovenduski, N. S., Orr, J. C., Palmieri, J., Santana-Falcón, Y., Schwinger, J., Séférian, R., Stock, C. A., Tagliabue, A., Takano, Y., Tjiputra, J., Toyama, K., Tsujino, H., Watanabe, M., Yamamoto, A., Yool, A., and Ziehn, T.: Twenty-first century ocean warming, acidification, deoxygenation, and upper-ocean nutrient and primary production decline from CMIP6 model projections, Biogeosciences, 17, 3439–3470, https://doi.org/10.5194/bg-17-3439-2020, 2020.

Mahowald, N. M., Muhs, D. R., Levis, S., Rasch, P. J., Yoshioka, M., Zender, C. S., and Luo, C.: Change in atmospheric mineral aerosols in response to climate: Last glacial period, preindustrial, modern, and doubled carbon dioxide climates: DUST RESPONSE TO CLIMATE, J. Geophys. Res. Atmospheres, 111, n/a-n/a, https://doi.org/10.1029/2005JD006653, 2006.

McMahon, P. B. and Chapelle, F. H.: Microbial production of organic acids in aquitard sediments and its role in aquifer geochemistry, Nature, 349, 233–235, https://doi.org/10.1038/349233a0, 1991.

Middelburg, J. J. and Levin, L. A.: Coastal hypoxia and sediment biogeochemistry, Biogeosciences, 6, 1273–1293, https://doi.org/10.5194/bg-6-1273-2009, 2009a.

Middelburg, J. J. and Levin, L. A.: Coastal hypoxia and sediment biogeochemistry, 1273–1293, 2009b.

Mills, M. M., Ridame, C., Davey, M., La Roche, J., and Geider, R. J.: Iron and phosphorus co-limit nitrogen fixation in the eastern tropical North Atlantic, Nature, 429, 292–294, https://doi.org/10.1038/nature02550, 2004.

Moore, J. K. and Braucher, O.: Sedimentary and mineral dust sources of dissolved iron to the world ocean, Biogeosciences, 5, 631–656, https://doi.org/10.5194/bg-5-631, 2008.

Moore, J. K., Doney, S. C., Kleypas, J. A., Glover, D. M., and Fung, I. Y.: An intermediate complexity marine ecosystem model for the global domain, Deep Sea Res. Part II Top. Stud. Oceanogr., 49, 403–462, https://doi.org/10.1016/S0967-0645(01)00108-4, 2001.

Moore, J. K., Doney, S. C., and Lindsay, K.: Upper ocean ecosystem dynamics and iron cycling in a global three-dimensional model: GLOBAL ECOSYSTEM-BIOGEOCHEMICAL MODEL, Glob. Biogeochem. Cycles, 18, n/a-n/a, https://doi.org/10.1029/2004GB002220, 2004.

Noffke, A., Hensen, C., Sommer, S., Scholz, F., Bohlen, L., Mosch, T., Graco, M., and Wallmann, K.: Benthic iron and phosphorus fluxes across the Peruvian oxygen minimum zone, Limnol. Oceanogr., 57, 851–867, https://doi.org/10.4319/lo.2012.57.3.0851, 2012.

Pham, A. L. D. and Ito, T.: Formation and Maintenance of the GEOTRACES Subsurface-Dissolved Iron Maxima in an Ocean Biogeochemistry Model, Glob. Biogeochem. Cycles, 32, 932–953, https://doi.org/10.1029/2017GB005852, 2018.

Pham, A. L. D. and Ito, T.: Ligand Binding Strength Explains the Distribution of Iron in the North Atlantic Ocean, Geophys. Res. Lett., 46, 7500–7508, https://doi.org/10.1029/2019GL083319, 2019.

Pozo Buil, M. and Di Lorenzo, E.: Decadal dynamics and predictability of oxygen and subsurface tracers in the California Current System, Geophys. Res. Lett., 44, 4204–4213, https://doi.org/10.1002/2017GL072931, 2017.

Qin, Q., Kinnaman, F. S., Gosselin, K. M., Liu, N., Treude, T., and Valentine, D. L.: Seasonality of water column methane oxidation and deoxygenation in a dynamic marine environment, Geochim. Cosmochim. Acta, 336, 219–230, https://doi.org/10.1016/j.gca.2022.09.017, 2022.

Reimers, C. E., Lange, C. B., Tabak, M., and Bernhard, J. M.: Seasonal spillover and varve formation in the Santa Barbara Basin, California, Limnol. Oceanogr., 35, 1577–1585, https://doi.org/10.4319/lo.1990.35.7.1577, 1990.

Renault, L., Deutsch, C., McWilliams, J. C., Frenzel, H., Liang, J.-H., and Colas, F.: Partial decoupling of primary productivity from upwelling in the California Current system, Nat. Geosci., 9, 505–508, https://doi.org/10.1038/ngeo2722, 2016.

Renault, L., McWilliams, J. C., Kessouri, F., Jousse, A., Frenzel, H., Chen, R., and Deutsch, C.: Evaluation of high-resolution atmospheric and oceanic simulations of the California Current System, Prog. Oceanogr., 195, 102564, https://doi.org/10.1016/j.pocean.2021.102564, 2021.

Sañudo-Wilhelmy, S., Kustka, A., Gobler, C., Hutchins, D., Yang, M., Lwiza, K., Burns, J., Raven, J., and Carpenter, E.: Phosphorus limitation of nitrogen fixation by Trichodesmium in the central Atlantic Ocean, Nature, 411, 66–9, https://doi.org/10.1038/35075041, 2001.

Severmann, S., McManus, J., Berelson, W. M., and Hammond, D. E.: The continental shelf benthic iron flux and its isotope composition, Geochim. Cosmochim. Acta, 74, 3984–4004, https://doi.org/10.1016/j.gca.2010.04.022, 2010.

Shchepetkin, A. F.: An adaptive, Courant-number-dependent implicit scheme for vertical advection in oceanic modeling, Ocean Model., 91, 38–69, https://doi.org/10.1016/j.ocemod.2015.03.006, 2015.

Shchepetkin, A. F. and McWilliams, J. C.: The regional oceanic modeling system (ROMS): a split-explicit, free-surface, topography-following-coordinate oceanic model, Ocean Model., 9, 347–404, https://doi.org/10.1016/j.ocemod.2004.08.002, 2005.

Shiller, A. M., Gieskes, J. M., and Brian Price, N.: Particulate iron and manganese in the Santa Barbara Basin, California, Geochim. Cosmochim. Acta, 49, 1239–1249, https://doi.org/10.1016/0016-7037(85)90013-4, 1985.

Sholkovitz, E. and Soutar, A.: Changes in the composition of the bottom water of the Santa Barbara Basin: effect of turbidity currents, Deep Sea Res. Oceanogr. Abstr., 22, 13–21, https://doi.org/10.1016/0011-7471(75)90014-5, 1975.

Sholkovitz, E. R. and Gieskes, J. M.: A PHYSICAL-CHEMICAL STUDY OF THE FLUSHING OF THE SANTA BARBARA BASIN1: FLUSHING OF THE SANTA BARBARA BASIN, Limnol. Oceanogr., 16, 479–489, https://doi.org/10.4319/lo.1971.16.3.0479, 1971.

Sigman, D. M., Robinson, R., Knapp, A. N., van Geen, A., McCorkle, D. C., Brandes, J. A., and Thunell, R. C.: Distinguishing between water column and sedimentary denitrification in the Santa Barbara Basin using the stable isotopes of nitrate, Geochem. Geophys. Geosystems, 4, https://doi.org/10.1029/2002GC000384, 2003.

Soetaert, K., Middelburg, J. J., Herman, P. M. J., and Buis, K.: On the coupling of benthic and pelagic biogeochemical models, Earth-Sci. Rev., 51, 173–201, https://doi.org/10.1016/S0012-8252(00)00004-0, 2000.

Sommer, S., Gier, J., Treude, T., Lomnitz, U., Dengler, M., Cardich, J., and Dale, A. W.: Depletion of oxygen, nitrate and nitrite in the Peruvian oxygen minimum zone cause an imbalance of benthic nitrogen fluxes, Deep Sea Res. Part Oceanogr. Res. Pap., 112, 113–122, https://doi.org/10.1016/j.dsr.2016.03.001, 2016.

Deleted: I,

Tagliabue, A., Sallée, J.-B., Bowie, A. R., Lévy, M., Swart, S., and Boyd, P. W.: Surface-water iron supplies in the Southern Ocean sustained by deep winter mixing, Nat. Geosci., 7, 314–320, https://doi.org/10.1038/ngeo2101, 2014.

Tagliabue, A., Aumont, O., DeAth, R., Dunne, J. P., Dutkiewicz, S., Galbraith, E., Misumi, K., Moore, J. K., Ridgwell, A., Sherman, E., Stock, C., Vichi, M., Völker, C., and Yool, A.: How well do global ocean biogeochemistry models simulate dissolved iron distributions?: GLOBAL IRON MODELS, Glob. Biogeochem. Cycles, 30, 149–174, https://doi.org/10.1002/2015GB005289, 2016.

Tagliabue, A., Bowie, A. R., Boyd, P. W., Buck, K. N., Johnson, K. S., and Saito, M. A.: The integral role of iron in ocean biogeochemistry, Nature, 543, 51–59, https://doi.org/10.1038/nature21058, 2017.

Testa, J. M., Brady, D. C., Di Toro, D. M., Boynton, W. R., Cornwell, J. C., and Kemp, W. M.: Sediment flux modeling: Simulating nitrogen, phosphorus, and silica cycles, Estuar. Coast. Shelf Sci., 131, 245–263, https://doi.org/10.1016/j.ecss.2013.06.014, 2013.

Till, C. P., Solomon, J. R., Cohen, N. R., Lampe, R. H., Marchetti, A., Coale, T. H., and Bruland, K. W.: The iron limitation mosaic in the California Current System: Factors governing Fe availability in the shelf/near-shelf region, Limnol. Oceanogr., 64, 109–123, https://doi.org/10.1002/lno.11022, 2019.

Treude, T., Smith, C. R., Wenzhöfer, F., Carney, E., Bernardino, A. F., Hannides, A. K., Krüger, M., and Boetius, A.: Biogeochemistry of a deep-sea whale fall: sulfate reduction, sulfide efflux and methanogenesis, Mar. Ecol. Prog. Ser., 382, 1–21, 2009.

Valentine, D. L., Fisher, G. B., Pizarro, O., Kaiser, C. L., Yoerger, D., Breier, J. A., and Tarn, J.: Autonomous Marine Robotic Technology Reveals an Expansive Benthic Bacterial Community Relevant to Regional Nitrogen Biogeochemistry, Environ. Sci. Technol., 50, 11057–11065, https://doi.org/10.1021/acs.est.6b03584, 2016.

Wallmann, K., José, Y. S., Hopwood, M. J., Somes, C. J., Dale, A. W., Scholz, F., Achterberg, E. P., and Oschlies, A.: Biogeochemical feedbacks may amplify ongoing and future ocean deoxygenation: a case study from the Peruvian oxygen minimum zone, Biogeochemistry, 159, 45–67, https://doi.org/10.1007/s10533-022-00908-w, 2022.

White, M. E., Rafter, P. A., Stephens, B. M., Wankel, S. D., and Aluwihare, L. I.: Recent Increases in Water Column Denitrification in the Seasonally Suboxic Bottom Waters of the Santa Barbara Basin, Geophys. Res. Lett., 46, 6786–6795, https://doi.org/10.1029/2019GL082075, 2019.

Widdows, J. and Brinsley, M.: Impact of biotic and abiotic processes on sediment dynamics and the consequences to the structure and functioning of the intertidal zone, J. Sea Res., 48, 143–156, https://doi.org/10.1016/S1385-1101(02)00148-X, 2002.

Deleted: Treude, T., Hamdan, L. J., Lemieux, S., Dale, A. W., and Sommer, S.: Rapid sulfur cycling in sediments from the Peruvian oxygen minimum zone featuring simultaneous sulfate reduction and sulfide oxidation, Limnol. Oceanogr., 66, 2661–2671, https://doi.org/10.1002/lno.11779, 2021.¶

Yao, M., Henny, C., and Maresca, J. A.: Freshwater Bacteria Release Methane as a By-Product of Phosphorus Acquisition, Appl. Environ. Microbiol., 82, 6994–7003, https://doi.org/10.1128/AEM.02399-16, 2016.

Yousavich, D. J., Robinson, D., Peng, X., Krause, S. J. E., Wenzhoefer, F., Janßen, F., Liu, N., Tarn, J., Kinnaman, F., Valentine, D. L., and Treude, T.: Marine anoxia initiates giant sulfur-bacteria mat proliferation and associated changes in benthic nitrogen, sulfur, and iron cycling in the Santa Barbara Basin, California Borderland, EGUsphere, 1–48, https://doi.org/10.5194/egusphere-2023-1198, 2023.

Zhou, Y., Gong, H., and Zhou, F.: Responses of Horizontally Expanding Oceanic Oxygen Minimum Zones to Climate Change Based on Observations, Geophys. Res. Lett., 49, e2022GL097724, https://doi.org/10.1029/2022GL097724, 2022.

Page 3: [1] Deleted Demarcus Robinson 10/30/23 9:28:00 PM

Page 7: [2] Deleted Demarcus Robinson 10/30/23 9:28:00 PM

Page 14: [3] Deleted Demarcus Robinson 10/30/23 9:28:00 PM

Page 18: [4] Deleted Demarcus Robinson 10/30/23 9:28:00 PM

Page 18: [4] Deleted Demarcus Robinson 10/30/23 9:28:00 PM

Page 18: [4] Deleted Demarcus Robinson 10/30/23 9:28:00 PM

Page 18: [5] Deleted Demarcus Robinson 10/30/23 9:28:00 PM

Page 18: [5] Deleted Demarcus Robinson 10/30/23 9:28:00 PM

Page 18: [6] Deleted Demarcus Robinson 10/30/23 9:28:00 PM

Page 19: [7] Deleted Demarcus Robinson 10/30/23 9:28:00 PM

Page 19: [7] Deleted Demarcus Robinson 10/30/23 9:28:00 PM

Page 19: [7] Deleted Demarcus Robinson 10/30/23 9:28:00 PM

Page 19: [7] Deleted Demarcus Robinson 10/30/23 9:28:00 PM

Page 19: [7] Deleted Demarcus Robinson 10/30/23 9:28:00 PM

Page 19: [7] Deleted Demarcus Robinson 10/30/23 9:28:00 PM

Page 19: [7] Deleted Demarcus Robinson 10/30/23 9:28:00 PM

Page 19: [7] Deleted Demarcus Robinson 10/30/23 9:28:00 PM

Page 19: [7] Deleted Demarcus Robinson 10/30/23 9:28:00 PM

Page 19: [7] Deleted Demarcus Robinson 10/30/23 9:28:00 PM

Page 19: [7] Deleted Demarcus Robinson 10/30/23 9:28:00 PM

Page 19: [7] Deleted Demarcus Robinson 10/30/23 9:28:00 PM

Page 19: [7] Deleted Demarcus Robinson 10/30/23 9:28:00 PM

Page 19: [7] Deleted **Demarcus Robinson** **10/30/23 9:28:00 PM**

Page 19: [7] Deleted **Demarcus Robinson** **10/30/23 9:28:00 PM**

Page 20: [8] Deleted **Demarcus Robinson** **10/30/23 9:28:00 PM**

Page 23: [9] Deleted **Demarcus Robinson** **10/30/23 9:28:00 PM**

Page 24: [10] Deleted **Demarcus Robinson** **10/30/23 9:28:00 PM**